Stony Brook University

Visual Synthesis of Planar Parallel Manipulators using Constraint Manifold Geometry

A Thesis Presented

by

Sagar Anantwar

to

The Graduate School

in partial fulfillment of the

Requirements

for the degree of

Master of Science

in

Mechanical Engineering

Stony Brook University

December 2011

Stony Brook University

The Graduate School

Sagar Anantwar

We, the thesis committee for the above candidate for the
Master of Science degree,
hereby recommend acceptance of this thesis.

Dr. Anurag Purwar, Advisor,
Research Assistant Professor, Mechanical Engineering Department

Dr. Q. Jeffrey Ge, Chairman of Thesis Committee
Professor, Mechanical Engineering Department

Dr. Yu Zhou,
Assistant Professor, Mechanical Engineering Department

This thesis is accepted by the Graduate School.

Lawerence Martin
Dean of the Graduate School

Abstract of the Thesis

Visual Synthesis of Planar Parallel Manipulators using Constraint Manifold Geometry

by

Sagar Anantwar

Master of Science

in

Mechanical Engeineering

Stony Brook University

2011

In this thesis, a visual approach for the dimensional synthesis of planar parallel manipulators is discussed. The presented approach transforms the kinematic constraint problem to a geometric constraint manifold manipulation problem.

For planar mechanisms, the kinematic constraint equations represent the limits for the motion of the links in the Cartesian space. The use of Quaternions is made in designing of this motion. The problem of motion of planar mechanisms is translated into a problem of designing of a smooth rational curve in the Quaternion space (Image space).

An intuitive graphical design tool has been developed. The design tool facilitates the user for synthesis of planar parallel manipulators. The design problem has been transformed into a problem of manipulation of surfaces so as to contain the curve in the volume between the surfaces, yielding the desired mechanism.

Contents

List of Figures

List of Tables

ACKNOWLEDGEMENTS

I take this opportunity to first thank my research advisor, Prof. Anurag Purwar, for his thorough guidance and invaluable support throughout my academic and research term at Stony Brook University. He has an extensive knowledge of the subject, which he willingly shared with me. It is because of him I have successfully been able to complete my research.

I would also like to extend my gratitude to Prof. Jeff Ge for agreeing to chair my thesis committee and Prof. Yu Zhou for being a member of the thesis committee.

I owe a lot to my parents and my sister as they have been my backbone and have stood by me throughout. I am indebted to them, all this would not have been possible without their encouragement and faith in my capabilities.

Last but not the least, my close friends at Stony Brook University made experience a memorable one, I cannot thank them enough.

As a graduate student of Stony Brook University, I have learned at lot and grown as a person, in the past one and half years. The environment here has been educating, inspiring and pleasant. I am now confident and well rounded in all specialities and have a vision of how I see myself grow in the future, I owe a lot to Prof. Anurag Purwar, my advisor and mentor.

Chapter 1

Introduction and Background

This thesis deals with the problem of dimensional synthesis of planar parallel manipulators via use of constraint manifold geometry. In this introductory chapter a general overview of the existing work in the area of dimensional synthesis of planar parallel manipulator, main contributions of this thesis, different optimization methods for synthesis of parallel manipulators and the issue of singularity are presented.

Mechanisms are basically classified into three kinds based on their purposes: 1. function generation, 2. path generation and 3. motion generation. This thesis is concerned with the dimensional synthesis of planar parallel manipulators for motion generation. A motion generation mechanism is a mechanism which guides a rigid body through the required positions via a rational motion. Rational motions are defined as a ratio of two polynomial functions and are compatible with the industry standard Non-Uniform Rational B-splines

(NURBS) based CAD/CAM systems.

A parallel manipulator consists of a moving platform that is connected to a base by several legs. Another definition is given by (Merlet 2006 [1]): a generalized parallel manipulator is a closed-loop kinematic chain mechanism whose end-effector is linked to the base by several independent kinematic chains.

Although it was Dr. Eric Gough [66] who invented the first variable-length octahedral hexapod in England in the 1950's, his parallel mechanism, also called tire-testing machine did not draw much public attention. Then in 1965, Stewart [67] presented his paper on the design of a flight simulator based upon a 6-DOF parallel platform. This work had a great impact on subsequent developments in the field of parallel mechanisms. Since then, many researchers have done much work on parallel mechanisms and both theoretical analyses and practical applications have been studied.

In the past two decades significant amount of research has been done in this field, evident from the application of well-known curve and surface design algorithms from computer aided geometric design(CAGD) to the field of theoretical kinematics for the purpose of developing rational Bezier and B-Spline motions of rigid bodies. The idea behind such a synergy is that the problem of designing rational curves in a higher dimensional projective space via a special mapping. By choosing the quaternion representation of the displacement and orientation, the problem is further reduced to designing curves in the space of quaternions. Rational motions, with applications spanning across areas such as motion animation in computer graphics, task specification in

mechanism synthesis, and virtual reality systems as well as Cartesian motion planning in robotics, are an attractive proposition since they integrate well the industry standard nonuniform rational B-spline(NURBS) based computer aided design/computer aided manufacturing(CAD/CAM) system. Furthermore, from a computational perspective they can easily exploit fast and stable algorithms from CAGD.

Theory of mechanism synthesis is well-developed (see Sandor and Erdman [40], Suh and Radcliffe [41], and McCarthy [42]), and there has been a great deal of academic research in the development of software systems for the synthesis of mechanisms (KINSYN III from Rubel and Kaufamn [27], LINCAGES from Erdman and colleagues [28, 29], Kihonge et al. [30], Spades from Larochelle [31], Perez and McCarthy [35], Su and McCarthy [36], Synthetica from Su et al. [37]). In the commercial domain, SyMech [38] and WATT [39] are two well-known software systems for planar mechanisms design.

Researchers have also done work in the direction of synthesis of parallel mechanisms considering the aspects of design such as optimization and singularity free work space. The work presented by Tsai and Kim [72] presents the designing of a 3-DOF 3-PRRR type Cartesian Parallel Manipulator. For designing of the manipulator they make use of the inverse kinematics and forward kinematics relations. Using the inverse kinematics relations, all the joint angles and the position vector for the second link are derived. Then, as each limb has a finite reach, the relations derived for the position vector are

subjected to constraints using the link length parameters. An this constraint equation is used for designing of the parallel manipulator. A similar kind of vector approach has been used by Tsai and Kim [73] for kinematic synthesis of 3-DOF 3-RPS parallel manipulators.

For designing of 3-RPS type parallel manipulators the approach presented by Rao N. and Rao K. [75] makes use of a hybrid design optimization method. The approach uses the vector equations used by Tsai and Kim [73], and the architectural parameters of the manipulator are determined by considering the design problem as an optimization problem. The hybrid method first carries out the global search for the solution using genetic algorithm and then applies the simplex method for the local search. While determining the dimensions of the fixed platform, the physical constraints such as limitation on the range of motion of the spherical joints are considered. The work presented by Arsenault [68] makes use of geometrical method for determination of the workspace and the optimization is done using genetic algorithms as they have good converging property.

The general approach of the work presented is closely related to the kinematic mapping approach for dimensional synthesis of planar and spherical mechanisms pioneered by Ravani and Roth [5]. Their work was followed by Bodduluri and McCarthy [15], Bodduluri [16], and Larochelle [17]. Their approach involved minimizing the distance error between the given positions and the image curve of the chain. This resulted in an approximate motion synthesis. Venkataramanujam and Larochelle [20] used parametrized constraint

manifolds and employed non-linear optimization to give numerical methods for approximate motion synthesis of open and closed chains.

To study the dimensional synthesis problem from the perspective of constrained motion interpolation, Jin and Ge [53] and Purwar and Jin [54] have studied the problem of motion interpolation under kinematic constraints for planar and spherical 6R closed chains. By using quaternions or dual quaternions and kinematic mapping approach, the problem of constrained motion interpolation was transformed into a problem of designing a rational curve constrained to satisfy geometry of the constraint manifold. Starting with an initial unconstrained curve, the curve was manipulated using an iterative numerical method until it fits inside the constraint manifold. The current work investigates the inverse problem, that is, to manipulate the constraint manifold while keeping the given rational curve fixed for dimensional synthesis. Jun et al. [25] initially designed and developed a system for the dimensional synthesis of planar 6R mechanisms, this system was then further developed to account for planar parallel manipulators by Purwar and Gupta [55]. This system was limited to the use of RRR and RPR configurations only, this work is an extension of that to account for all the different configurations.

The design method treats a planar parallel manipulator as an assembly of three open chains connected to a moving platform. Each open chain imposes kinematic constraints that limit the positions and orientations of the object connected to the end link. We use the algebraic form of the constraint manifold for the planar open chains. Thus, the kinematic constraints are transformed

into geometric constraints, and the given rational motion is transformed into a rational curve in the image space. This way, the problem reduces to finding the constraint manifold that accommodates the given rational curve. These constraint manifolds can be manipulated so as to change their location, orientation, and the mean curvature. Algebraically, the kinematic constraints are derived in the inequality form, where the limits of the inequalities are functions of link lengths, while the constraint functions themselves incorporate parameters that describe the location and orientation of fixed and moving frames. In the end, we design open chains that simultaneously satisfy the kinematic constraints and the motion requirements. A visual interpretation of this approach is that, we find the smallest possible pair of constraint manifolds that will contain the given image curve entirely in the volume between them.

The work presented can be used for synthesis of mechanisms and for trajectory verification. For trajectory verification, the designer can just input the mechanism parameters available and the desired motion of the moving platform, and upon inputting of these parameters, if the interpolated image curve is fully contained in the volume between the pair of constraint manifolds for each leg configuration, it can be validated that the mechanism will be able to perform the desired task.

In addition to the synthesis of mechanisms optimization is a very important part while synthesis of mechanisms. Many researchers have used different methods. Gosselin [69] presented a non-linear optimization method by identification of relevant design parameters and objective functions for parasitic

motion minimization of spatial parallel manipulators. Similar kind of optimization technique was presented by Ceccarelli, Carbone and Ottaviano [70], where a function was derived based on the desired parameters and the function was optimized subjected to some constraints.

Mechanism consists of some spaces in its workspace where the mechanism does not perform naturally, these areas are called as singularity spaces. In the dimensional synthesis of planar parallel mechanisms, singularity of mechanisms [58] has a large effect on the synthesis of mechanisms. A singular configuration is a special configuration in which the parallel mechanism gains an uncontrollable freedom. For parallel manipulators, there are different singularity conditions based on the analysis of the Jacobian matrix that is formed from the line of action of the leg connectors [63].

There are three types of singularities as stated by both Tsai [62] and Merlet [1] based on the Jacobian Matrix analysis: the inverse kinematic singularity, where the manipulator loses one or more degrees of freedom; the direct kinematic singularity, where the platform gains additional degree(s) of freedom; and the combined singularities. Other researchers [65] found some more kind of singularities called architecture singularities, where the parallel manipulator configuration exhibits a continuous motion with all actuators fixed; formulation singularity and configuration singularity. In this thesis we do not deal with the problem of singularity, and the focus has been on the design problem.

The rest of the thesis is organized as follows. Chapter 2 deals with kinematic constraint equations and manifolds of planar parallel manipulator. Chap-

Figure 1.1: A 3-RRR planar parallel manipulator. Source: Institute of Mechatronic systems, Liebniz Universität Hannover

ter 3 is a guide to use the software tool developed for dimensional synthesis. The final chapter summarizes the work of this research and discusses some of the limitations of this work.

Chapter 2

Constraint Manifold for Planar Parallel Manipulator

2.1 Introduction

This chapter deals with the formulation of the kinematic constraints of planar parallel manipulators using quaternion based representation found in McCarthy [7] and Ge [56].

The organization of the chapter is as follows. Section 2.2 explains the classification of different open chains used as the legs for planar parallel manipulators, section 2.3 explains planar displacements and planar quaternions, and section 2.4 explains the derivation and kinematic constraint equation and manifolds for the different types of planar open chains.

2.2 Classification of Open Chains used as Legs in a 3-Legged Planar Parallel Manipulators

A three legged parallel manipulator is a 3 DOF closed loop kinematic chain whose end effectors are linked to a base platform by three independent 3 DOF open loop kinematic chains. Each open loop chain has one active joint and two passive joints. Each chain consists of two types of joints Revolute(R) and Prismatic(P) [23].

The possible combinations of Revolute(R) and Prismatic(P) joints in an 3-legged open loop chain are:

RRR, RPR, RRP, PRR, PRP, PPR, RPP

The PPP chain is not useful and must be excluded as it gives rise to only translation with no change in orientation. Thus, there are seven possible useful open loop kinematic chains.

For a 3 DOF open chain mechanism, there exists one active joint (actuated) and two passive joints. This active joint is represented with an underscore. There are 21 3-DOF legs in total (Table 2.2) [58]. The three configurations represented with a cross mark (marked with ^{X}) do not yield 3-DOF planar parallel manipulators (they contain only one controllable DOF). Also, there are eight pairs of symmetric legs, where each pair leads to two kinematically equivalent planar parallel manipulators. Therefore, these eight legs are elimi-

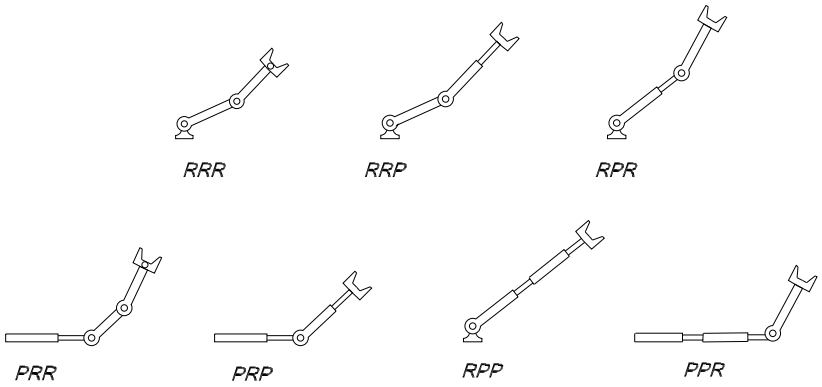

Figure 2.1: All possible useful 3 DOF mechanisms

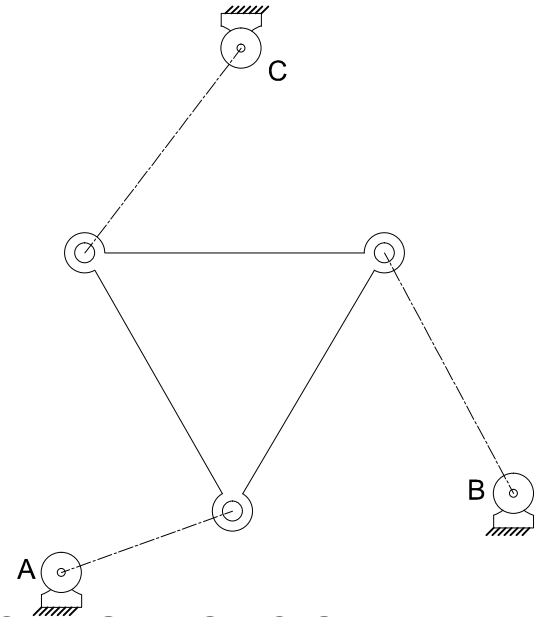

Figure 2.2: A Planar Parallel Manipulator

nated (marked with ˜), which leaves us with only ten configurations.

Table 2.1: All possible 3-DOF planar legs

$\underline{\mathrm{R}}\mathrm{RR}$	$\underline{\mathrm{R}}\mathrm{PR}$	$\underline{\mathrm{R}}\mathrm{PP}^X$	$\underline{\mathrm{P}}\mathrm{RR}$	$\underline{\mathrm{P}}\mathrm{RP}$	$\underline{\mathrm{P}}\mathrm{PR}$	$\underline{\mathrm{R}}\mathrm{RP}$
$\mathrm{R}\underline{\mathrm{R}}\mathrm{R}$	$\mathrm{R}\underline{\mathrm{P}}\mathrm{R}$	$\mathrm{R}\underline{\mathrm{P}}\mathrm{P}$	$\mathrm{P}\underline{\mathrm{R}}\mathrm{R}$	$\mathrm{P}\underline{\mathrm{R}}\mathrm{P}^X$	$\mathrm{P}\underline{\mathrm{P}}\mathrm{R}^{\sim}$	$\mathrm{R}\underline{\mathrm{R}}\mathrm{P}^{\sim}$
$\mathrm{RR}\underline{\mathrm{R}}^{\sim}$	$\mathrm{RP}\underline{\mathrm{R}}^{\sim}$	$\mathrm{RP}\underline{\mathrm{P}}^{\sim}$	$\mathrm{PR}\underline{\mathrm{R}}^{\sim}$	$\mathrm{PR}\underline{\mathrm{P}}^{\sim}$	$\mathrm{PP}\underline{\mathrm{R}}^X$	$\mathrm{RR}\underline{\mathrm{P}}^{\sim}$

2.3 Planar Displacements and Planar Quaternions

A planar displacement can be represented by a planar quaternion (see Bottema and Roth [6] and McCarthy [7]). Planar quaternions have been used for designing planar open chains (Ravani and Roth [4], Larochelle [60], Murray et al. [24], Perez and McCarthy [59]).

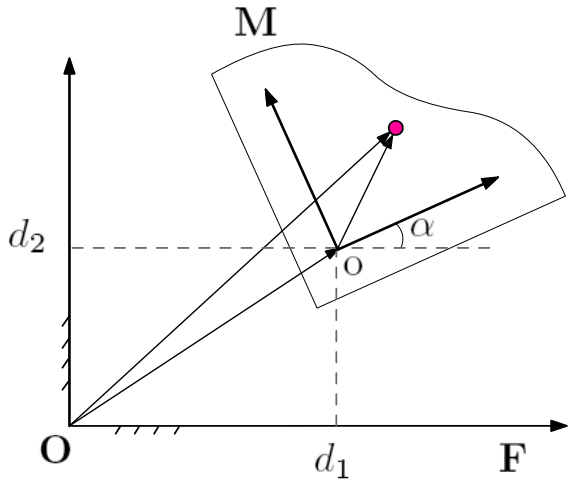

Figure 2.3: A planar displacement.

For a planar displacement shown in Fig. (2.3), let d_1, d_2 denote the coordinates of the origin of the moving frame **M** in the fixed frame **F** and α

denote the rotation angle of $\mathbf{M}$ relative to $\mathbf{F}$. Then a planar displacement can be represented by a planar quaternion, $\mathbf{Z} = Z_1\epsilon\mathbf{i} + Z_2\epsilon\mathbf{j} + Z_3\epsilon\mathbf{k} + Z_4$, where ($\mathbf{i}$, $\mathbf{j}$, $\mathbf{k}$, 1) form the quaternion basis and ϵ is the dual unit with the property $\epsilon^2 = 0$. The components of the planar quaternion, $\mathbf{Z} = (Z_1,\ Z_2,\ Z_3,\ Z_4)$, are given by

$$\begin{aligned} Z_1 &= (d_1/2)\cos(\alpha/2) + (d_2/2)\sin(\alpha/2), \\ Z_2 &= -(d_1/2)\sin(\alpha/2) + (d_2/2)\cos(\alpha/2), \\ Z_3 &= \sin(\alpha/2), \\ Z_4 &= \cos(\alpha/2). \end{aligned} \tag{2.1}$$

These four components can be identified as co-ordinates of a point in four dimensional space. The point $\mathbf{Z}$ is called the *image point of a planar displacement*. The set of image points that represent all planar displacements is called the *image space* of planar displacements and is denoted as Σ_p. In view of Eq.(2.1), the coordinates of an image point must satisfy the equation:

$$Z_3^2 + Z_4^2 = 1. \tag{2.2}$$

The above equation may be interpreted as defining a hyper-circular cylinder in four dimensions.

If the point $\mathbf{x}$ in $\mathbb{R}^2$ is identified with $\mathbf{x} = y\mathbf{i}\epsilon - x\mathbf{i}\epsilon + \mathbf{k}$, then the result of planar displacement of $\mathbf{x}$ is obtained by

$$\mathbf{X} = \mathbf{Z}\mathbf{x}\mathbf{Z}^*, \tag{2.3}$$

where $\mathbf{Z} = Z_4 - Z_1\epsilon\mathbf{i} - Z_2\epsilon\mathbf{j} - Z_3\mathbf{k}$ is the *conjugate* of $\mathbf{Z}$.

We can use homogeneous transform matrix to represent Eq.(2.3)

$$\begin{bmatrix} \mathbf{X} \\ 1 \end{bmatrix} = [A] \begin{bmatrix} \mathbf{x} \\ 1 \end{bmatrix}, \tag{2.4}$$

where

$$[A] = \frac{1}{Z_3^2 + Z_4^2} \begin{bmatrix} Z_4^2 - Z_3^2 & -2Z_3Z_4 & 2(Z_1Z_4 - Z_2Z_3) \\ 2Z_3Z_4 & Z_4^2 - Z_3^2 & 2(Z_1Z_3 + Z_2Z_4) \\ 0 & 0 & Z_3^2 + Z_4^2 \end{bmatrix}. \tag{2.5}$$

Note that when Z_i $(i = 1, 2, 3, 4)$ is replaced by wZ_i, where w is a non-zero scalar, the matrix $[A]$ is unchanged. From this perspective, the four components of a planar quaternion can also be considered as a set of homogeneous coordinates for a planar displacement.

Quaternion algebra is also used for composing two successive planar displacements. Let $\mathbf{Z}_0, \mathbf{Z}_1$ denote two planar displacements. The composition of two planar displacements $\mathbf{Z}_1$ followed by $\mathbf{Z}_0$ is given by the quaternion product $\mathbf{Z}_0\mathbf{Z}_1$.

2.4 Kinematic Constraint Equations and Manifolds of Planar Open Chains

In this section, the kinematic constraint equations for all the seven planar open chain configurations (RRR, RPR, RRP, PPR, PRR, PRP, RPP) have been derived, and their standard form along with the constraint manifolds representing these kinematic constraint equations have been shown.

Originally these equations were derived by Aditya (see Jin[57], and Purwar, Gupta[55]), but except for configurations RRR, and RPR rest of the cases were not in a form that could be used for geometric representation. Later, Ping ([61]), re-derived the remaining five cases and implemented them in *Mathematica*.

2.4.1 Planar RRR Open Chain

Consider a planar RRR open chain as shown in Fig. 2.4. The length of the first link is a, the length of the second link is b and θ, ϕ, ψ are joint angles for three revolute joints respectively. In the figure, **F** and **M** mark the fixed and the moving frames, respectively. The fixed pivot is located at (x, y), while the moving frame is located at a distance of h from the end pivot. The moving frame is assumed to be tilted by angle of α from the line joining the end pivot and the origin of the moving frame. When the fixed and moving frames are located at A and B respectively the parametrized equation of the constraint manifold $\mathbf{Z}(\theta, \phi, \psi)$ of a RRR robot open chain is obtained as follows:

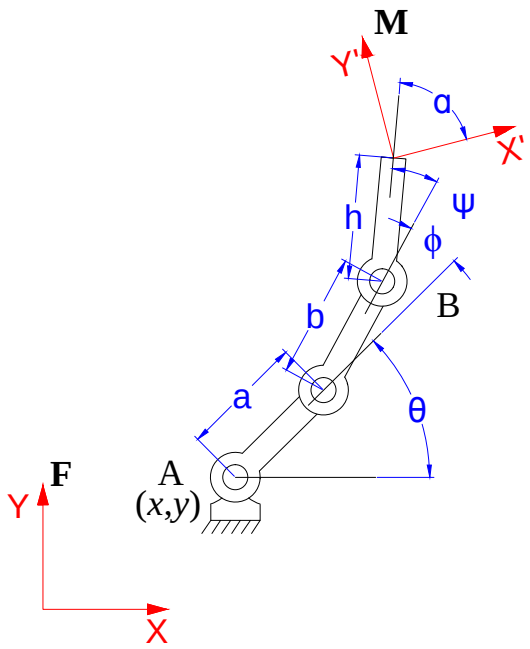

Figure 2.4: A planar RRR open chain

$$\mathbf{Z}(\theta, \phi, \psi) = \mathbf{Z}(\theta)\mathbf{X}(a)\mathbf{Z}(\phi)\mathbf{X}(b)\mathbf{Z}(\psi). \tag{2.6}$$

The coordinates of $\mathbf{Z}(\theta, \phi, \psi) = (Z_1, Z_2, Z_3, Z_4)$ can be obtained as:

$$\begin{aligned} Z_1 &= a/2\cos(\theta - \phi - \psi)/2 + b/2\cos(\theta + \phi - \psi)/2, \\ Z_2 &= a/2\sin(\theta - \phi - \psi)/2 + b/2\sin(\theta + \phi - \psi)/2, \\ Z_3 &= \sin(\theta + \phi + \psi)/2, \\ Z_4 &= \cos(\theta + \phi + \psi)/2. \end{aligned} \tag{2.7}$$

From Eq.(2.7), it can be seen that the coordinates, Z_i, satisfy the following

equations:

$$Z_1^2 + Z_2^2 = a^2/4 + b^2/4 + (ab/2)\cos(\phi). \tag{2.8}$$

$$Z_3^2 + Z_4^2 = 1. \tag{2.9}$$

Since the range of $\cos(\phi)$ is [-1 1], Eq.(2.8) can be reduced to:

$$(a-b)^2/4 \leq Z_1^2 + Z_2^2 \leq (a+b)^2/4. \tag{2.10}$$

The variables θ and ψ can be eliminated from Eq.(2.7) to yield the following equation:

$$4Z_1^2 + 4Z_2^2 - Z_3^2(a^2 + b^2 + 2ab\cos\phi) - Z_4^2(a^2 + b^2 + 2ab\cos\phi) = 0 \tag{2.11}$$

$a^2 + b^2 + 2ab\cos\phi$ is the square of the distance between the base joint and third joint. Let it be denoted by R. Thus the equation becomes:

$$Z_1^2 + Z_2^2 - \frac{R^2}{4}Z_3^2 - \frac{R^2}{4}Z_4^2 = 0 \tag{2.12}$$

Let the points of R^4 be denoted x=(x,y,z,w) so the above equation can be written as:

$$x^2 + y^2 - \frac{R^2}{4}z^2 - \frac{R^2}{4}w^2 = 0 \tag{2.13}$$

This can be written in the quadratic form as:

$$x^T[Q]x = 0 \tag{2.14}$$

with the coefficient matrix as:

$$Q = \begin{bmatrix} 1 & 0 & 0 & 0 \\ 0 & 1 & 0 & 0 \\ 0 & 0 & -\frac{R^2}{4} & 0 \\ 0 & 0 & 0 & -\frac{R^2}{4} \end{bmatrix} \tag{2.15}$$

As shown in the Figure 2.4 a general choice of fixed and moving reference planes transforms the coefficient matrix to the form below:

$$[Q'] = [C^{-1}]^T[Q][C^{-1}] \tag{2.16}$$

where, $[C] = [G^+][H^-]$ is the matrix form of the quaternion transformation to the new fixed and moving frames.

$$[G] = (x/2, y/2, 0, 1), \tag{2.17}$$
$$[H] = (h/2\cos(\alpha)/2, -h/2\sin(\alpha)/2, \sin(\alpha)/2, \cos(\alpha)/2)$$

$$\mathbf{Z}'(\theta, \phi, b)[Q']\mathbf{Z}(\theta, \phi, b) = 0 \tag{2.18}$$

Simplifying the above equation we get:

which gives the following equation:

$$(Z_4^2 - Z_3^2)(\sigma_1 + \sigma_2) + 2Z_3Z_4(\tau_2 - \tau_1) + Z_1Z_3\cos\alpha \tag{2.19}$$

$$-Z_1Z_4sin\alpha - Z_2Z_3sin\alpha - Z_2Z_4cos\alpha = 0 \tag{2.20}$$

Simplifying Eq.(2.19)

$$F(Z_1, Z_2, Z_3, Z_4) = \frac{(Z_1 - \sigma_1 Z_3 - \tau_1 Z_4)^2 + (Z_2 - \sigma_2 Z_3 - \tau_2 Z_4)^2}{Z_3^2 + Z_4^2}, \text{and} \tag{2.21}$$

$$\begin{aligned} \sigma_1 &= (y + h\sin\alpha)/2, & \tau_1 &= (x + h\cos\alpha)/2, \\ \sigma_2 &= (-x + h\cos\alpha)/2, & \tau_2 &= (y - h\sin\alpha)/2. \end{aligned} \tag{2.22}$$

$$\frac{(a-b)^2}{4} \leq F(Z_1, Z_2, Z_3, Z_4) \leq \frac{(a+b)^2}{4}, \tag{2.23}$$

Eq.(2.23) characterize the kinematic constraints of a planar RRR open chain and define the constraint manifold for the chain.

Thus, the constraint manifold of the planar RRR closed chains is given by a pair of concentric and co-oriented sheared hyperboloid and for the a mechanism to pass through a given motion, the image curve would have to be contained between the constraint manifolds.

Using the projective property of the planar quaternion, to visualize the hyper-geometric shape described by Eq.(2.23), we observe its intersection

with the hyperplane $Z_4 = 1$; in the other words, we project Eq.(2.23) onto hyperplane$Z_4 = 1$. Denote $(z_1, z_2, z_3, 1)$ as the projected point of (Z_1, Z_2, Z_3, Z_4), both of which represent the same planar displacement. Then, it is yielded that

$$F(z_1, z_2, z_3, 1) = \frac{(z_1 - \sigma_1 z_3 - \tau_1)^2 + (z_2 - \sigma_2 z_3 - \tau_2)^2}{z_3^2 + 1} \tag{2.24}$$

where σ_1, σ_2, τ_1 and τ_2 are the same as Eq.(2.22).

The volume field described by Eq.(2.24) creates implicit surfaces of (z_1, z_2, z_3). The means to develop the isosurface is to, without loss of generality, set $F(z_1, z_2, z_3, 1) = c$, $c \in [L_{\min}^2/4, L_{\max}^2/4]$, and to be standard, we also reorganize Eq.(2.24) to Eq.(2.25)

$$\frac{(z_1 - \sigma_1 z_3 - \tau_1)^2}{c} + \frac{(z_2 - \sigma_2 z_3 - \tau_2)^2}{c} - z_3^2 = 1 \tag{2.25}$$

This is a typical sheared a circular hyperboloid in the projective (z_1, z_2, z_3) space. See Table 2.2. The hyperboloid centralizes at $(\tau_1, \tau_2, 0)$. The central axis is $\frac{z_1 - \tau_1}{\sigma_1} = \frac{z_2 - \tau_2}{\sigma_2} = \frac{z_3}{1}$, so that the hyperboloid orients along the vector$(\sigma_1, \sigma_2, 1)$. It is evident to tell that the center and the orientation are decided by the location of the fixed pivot, the length of the floating link and the relative angle of $\mathbf{M}$ to the floating link. Besides, the intersection circle of the hyperboloid with the plane $z_3 = 0$ has a radius, r, equal to $\sqrt{c}$, which determines the size of the hyperboloid; the greater is c, the larger is the size of the hyperboloid. While the value of $F(z_1, z_2, z_3, 1)$ is varying from the lower boundary to the ceiling, except that the size of the hyperbolic manifold in-

Table 2.2: Parameters for the projective sheared hyperboloid presented by equation (2.25)

Geometric Features	Constraint Parameters
Center	$(\tau_1, \tau_2, 0)$
Orientation	$(\sigma_1, \sigma_2, 1)$
Intersected Circle	$\frac{L_{\min}}{2} \leq r = \sqrt{c} \leq \frac{L_{\max}}{2}$

creases correspondingly, the center and the orientation keep stationary.

The implicit surfaces is a set of concentric and co oriented sheared projective hyperboloid. The hyperboloid set occupies the space bounded by an interior and an exterior hyperboloid in the projective image. Eq.(2.25). A representation of the pair of sheared hyperboloids implemented in Mathematica are shown in Fig. (2.5).

2.4.1.1 Inverse Kinematics for Planar RRR Open Chain

The inverse kinematics problem is stated: Given the end-effector pose $\{X, Y, \delta\}^T$, calculate the three actuated joint (R or P) values [71]. In the case of an RRR open chain, the joint variables to be calculated are θ, ϕ and ψ. The notations used in the inverse kinematic relations are given below:

A_x, A_y are the $x-$coordinate and $y-$coordinate of point A.

B_x, B_y are the $x-$coordinate and $y-$coordinate of point B.

a, b, and h are the link lengths of first link, second link and coupler link.

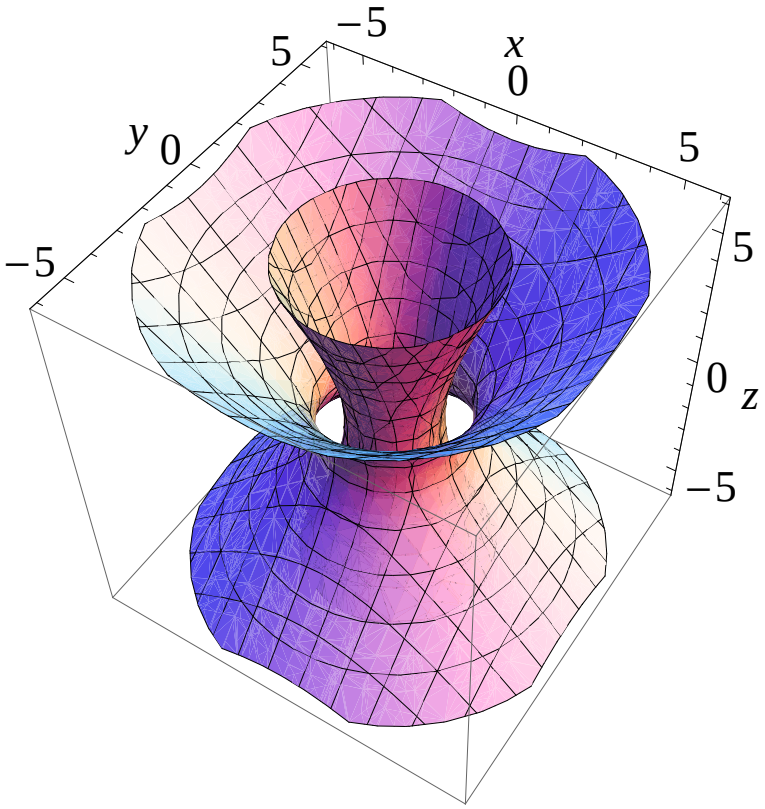

Figure 2.5: A pair of sheared hyperboloids representing a pair of constraint manifolds for an RRR open chain.

$$\begin{aligned} B_x &= X - h\cos(\delta + \alpha), \\ B_y &= Y - h\sin(\delta + \alpha) \end{aligned} \tag{2.26}$$

The joint angles can be calculated using the following relations:

$$\theta = 2\tan^{-1}\left(\frac{-F \pm \sqrt{E^2 + F^2 - G^2}}{G - E}\right) \tag{2.27}$$

$$\phi = \tan^{-1}\left(\frac{B_y - A_y - a\sin(\theta)}{B_x - A_x - a\cos(\theta)}\right) - \theta \tag{2.28}$$

$$\psi = \delta - \alpha - \theta - \phi \tag{2.29}$$

Where, the values of E, F,and G are given by the following relations:

$$\begin{aligned} E &= 2(B_x - A_x)a, \\ F &= 2(B_y - A_y)a, \\ G &= b^2 - a^2 - (B_x - A_x)^2 - (B_y - A_y)^2. \end{aligned} \tag{2.30}$$

2.4.2 Planar RPR Open Chain

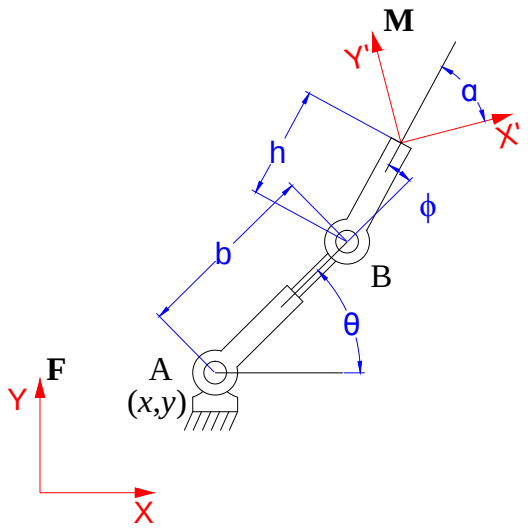

Figure 2.6: A planar RPR open chain

Consider a planar RPR open chain as shown in Fig. 2.6. The length of the first link is b and θ and ϕ are joint angles for two revolute joints respectively. In the figure, **F** and **M** mark the fixed and the moving frames, respectively. The fixed pivot is located at (x, y), while the moving frame is located at a distance of h from the end pivot. The moving frame is assumed to be tilted by angle of α from the line joining the end pivot and the origin of the moving frame. When the fixed and moving frames are located at A and B respectively the parametrized equation of the constraint manifold $\mathbf{Z}(\theta, b, \phi)$ of a RPR open chain is obtained as follows:

$$\mathbf{Z}(\theta, b, \phi) = \mathbf{Z}(\theta)\mathbf{X}(b)\mathbf{Z}(\phi). \tag{2.31}$$

The coordinates of $\mathbf{Z}(\theta, \phi, \psi) = (Z_1, Z_2, Z_3, Z_4)$ can be obtained as:

$$\begin{aligned} Z_1 &= b/2\cos(\theta - \phi)/2, \\ Z_2 &= b/2\sin(\theta - \phi)/2, \\ Z_3 &= \sin(\theta + \phi)/2, \\ Z_4 &= \cos(\theta + \phi)/2. \end{aligned} \tag{2.32}$$

From Eq.(2.32), it can be seen that the coordinates, Z_i, satisfy the following equations:

$$Z_1^2 + Z_2^2 = b^2/4 \tag{2.33}$$

$$Z_3^2 + Z_4^2 = 1. \tag{2.34}$$

Eq.(2.33) we get:

$$b_1^2/4 \leq Z_1^2 + Z_2^2 = b^2/4 \leq b_2^2/4. \tag{2.35}$$

This can be written in the quadratic form as:

$$x^T[Q]x = 0 \tag{2.36}$$

with the coefficient matrix as:

$$Q = \begin{bmatrix} 1 & 0 & 0 & 0 \\ 0 & 1 & 0 & 0 \\ 0 & 0 & 0 & 0 \\ 0 & 0 & 0 & 0 \end{bmatrix} \tag{2.37}$$

As shown in the Fig. (2.6) a general choice of fixed and moving reference planes transforms the coefficient matrix to the form below:

$$[Q'] = [C^{-1}]^T[Q][C^{-1}] \tag{2.38}$$

where, $[C] = [G^+][H^-]$ is the matrix form of the quaternion transformation to the new fixed and moving frames.

$$[G] = (x/2, y/2, 0, 1), \tag{2.39}$$
$$[H] = (h/2\cos(\alpha)/2, -h/2\sin(\alpha)/2, \sin(\alpha)/2, \cos(\alpha)/2)$$

$$\mathbf{Z}'(\theta, \phi, b)[Q']\mathbf{Z}(\theta, \phi, b) = 0 \tag{2.40}$$

Simplifying the above equation we get:

$$(Z_4^2 - Z_3^2)(\sigma_1 + \sigma_2) + 2Z_3Z_4(\tau_2 - \tau_1) + Z_1Z_3\cos\alpha \tag{2.41}$$

$$-Z_1Z_4sin\alpha - Z_2Z_3sin\alpha - Z_2Z_4cos\alpha = b^2/4 \tag{2.42}$$

Simplifying Eq.(2.41)

$$F(Z_1, Z_2, Z_3, Z_4) = \frac{(Z_1 - \sigma_1 Z_3 - \tau_1 Z_4)^2 + (Z_2 - \sigma_2 Z_3 - \tau_2 Z_4)^2}{Z_3^2 + Z_4^2}, \text{and} \tag{2.43}$$

$$\begin{aligned} \sigma_1 &= (y + h\sin\alpha)/2, & \tau_1 &= (x + h\cos\alpha)/2, \\ \sigma_2 &= (-x + h\cos\alpha)/2, & \tau_2 &= (y - h\sin\alpha)/2. \end{aligned} \tag{2.44}$$

$$\frac{b_1^2}{4} \leq F(Z_1, Z_2, Z_3, Z_4) \leq \frac{b_2^2}{4}, \tag{2.45}$$

Eq.(2.45) characterize the kinematic constraints of a planar RPR open

chain and define the constraint manifold for the chain.

Thus, the constraint manifold of the planar RPR closed chains is given by a pair of concentric and co-oriented sheared hyperboloids and for the a mechanism to pass through a given motion, the image curve would have to be contained between the constraint manifolds.

Using the projective property of the planar quaternion, to visualize the hyper-geometric shape described by Eq.(2.45), we observe its intersection with the hyperplane $Z_4 = 1$; in the other words, we project Eq.(2.45) onto hyperplane$Z_4 = 1$. Denote $(z_1, z_2, z_3, 1)$ as the projected point of (Z_1, Z_2, Z_3, Z_4), both of which represent the same planar displacement. Then, it is yielded that

$$F(z_1, z_2, z_3, 1) = \frac{(z_1 - \sigma_1 z_3 - \tau_1)^2 + (z_2 - \sigma_2 z_3 - \tau_2)^2}{z_3^2 + 1} \tag{2.46}$$

where σ_1, σ_2, τ_1 and τ_2 are the same as Eq.(2.44).

The volume field described by Eq.(2.46) creates implicit surfaces of (z_1, z_2, z_3). The means to develop the isosurface is to, without loss of generality, set $F(z_1, z_2, z_3, 1) = c$, $c \in [L_{\min}^2/4, L_{\max}^2/4]$, and to be standard, we also reorganize Eq.(2.46)

$$\frac{(z_1 - \sigma_1 z_3 - \tau_1)^2}{c} + \frac{(z_2 - \sigma_2 z_3 - \tau_2)^2}{c} - z_3^2 = 1 \tag{2.47}$$

This is a typical sheared a circular hyperboloid in the projective (z_1, z_2, z_3) space. See Table (2.3). The hyperboloid centralizes at $(\tau_1, \tau_2, 0)$. The central axis is $\frac{z_1 - \tau_1}{\sigma_1} = \frac{z_2 - \tau_2}{\sigma_2} = \frac{z_3}{1}$, so that the hyperboloid orients along the

vector$(\sigma_1, \sigma_2, 1)$. It is evident to tell that the center and the orientation are decided by the location of the fixed pivot, the length of the floating link and the relative angle of $\mathbf{M}$ to the floating link. Besides, the intersection circle of the hyperboloid with the plane $z_3 = 0$ has a radius, r, equal to $\sqrt{c}$, which determines the size of the hyperboloid; the greater is c, the larger is the size of the hyperboloid. A representation of the pair of sheared hyperboloids implemented in Mathematica are shown in Fig. (2.7).

Table 2.3: Parameters for the projective sheared hyperboloid presented by Eq.(2.47)

Geometric Features	Constraint Parameters
Center	$(\tau_1, \tau_2, 0)$
Orientation	$(\sigma_1, \sigma_2, 1)$
Intersected Circle	$\frac{L_{\min}}{2} \leq r = \sqrt{c} \leq \frac{L_{\max}}{2}$

2.4.2.1 Inverse Kinematics for Planar RPR Open Chain

The inverse kinematics problem is stated: Given the end-effector pose $\{X, Y, \delta\}^T$, calculate the three actuated joint (R or P) values [71]. In the case of an RPR open chain, the joint variables to be calculated are θ, b and ϕ. The notations used in the inverse kinematic relations are the same as used for the RRR open chain. The joint angles can be calculated using the following relations:

$$\theta = 2\tan^{-1}\left(\frac{-F \pm \sqrt{E^2 + F^2 - G^2}}{G - E}\right) \tag{2.48}$$

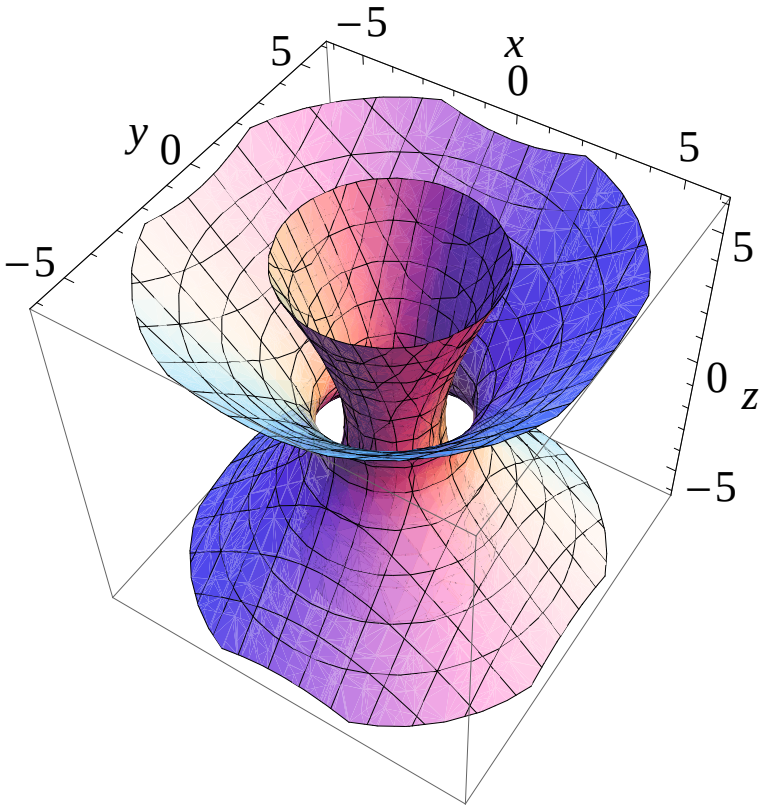

Figure 2.7: A pair of sheared hyperboloids representing a pair of constraint manifolds for an RPR open chain.

$$b = \frac{B_x - A_x}{\cos(\theta)} \tag{2.49}$$

$$\phi = \delta - \alpha - \theta \tag{2.50}$$

Where, the values of E, F,and G are given by the following relations:

$$\begin{aligned} E &= 2(B_x - A_x)b, \\ F &= 2(B_y - A_y)b, \\ G &= -b^2 - (B_x - A_x)^2 - (B_y - A_y)^2. \end{aligned} \tag{2.51}$$

2.4.3 Planar RRP Open Chain

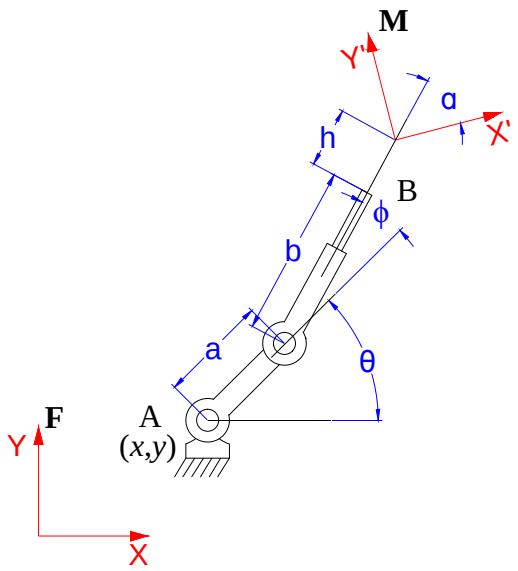

Figure 2.8: A planar RRP open chain

Consider a planar RRP open chain as shown in Fig. (2.8). The length of the first link is a, length of the second link is b and θ and ϕ are joint angles for two revolute joints respectively. In the figure, **F** and **M** mark the fixed and the moving frames, respectively. The fixed pivot is located at (x, y), while the moving frame is located at a distance of h from the end of link b. The moving

frame is assumed to be tilted by angle of α from the line joining the end pivot and the origin of the moving frame. When the fixed and moving frames are located at A and B respectively the parametrized equation of the constraint manifold $\mathbf{Z}(\theta, \phi, b)$ of a RRP open chain is obtained as follows:

$$\mathbf{Z}(\theta, b, \phi) = \mathbf{Z}(\theta)\mathbf{X}(a)\mathbf{Z}(\phi)\mathbf{X}(b). \tag{2.52}$$

The coordinates of $\mathbf{Z}(\theta, \phi, b) = (Z_1, Z_2, Z_3, Z_4)$ can be obtained as:

$$\begin{aligned} Z_1 &= b/2\cos(\theta+\phi)/2 + a/2\cos(\theta-\phi)/2, \\ Z_2 &= b/2\sin(\theta+\phi)/2 + a/2\sin(\theta-\phi)/2, \\ Z_3 &= \sin(\theta+\phi)/2, \\ Z_4 &= \cos(\theta+\phi)/2. \end{aligned} \tag{2.53}$$

From Eq.(2.53), it can be seen that the coordinates, Z_i, satisfy the following equations:

$$Z_1Z_4 + Z_2Z_3 = (b/2) + (a/2)\cos(\phi) \in [\tfrac{b_1-a}{2}, \tfrac{b_2+a}{2}] \tag{2.54}$$

$$Z_3^2 + Z_4^2 = 1. \tag{2.55}$$

From Eq.(2.54) we get the quadratic form as:

$$\frac{b_1 - a}{2} \leq x^T[Q]x \leq \frac{b_2 + a}{2}. \tag{2.56}$$

with the coefficient matrix as:

$$Q = \begin{bmatrix} 0 & 0 & 0 & 1/2 \\ 0 & 0 & 1/2 & 0 \\ 0 & 1/2 & 0 & 0 \\ 1/2 & 0 & 0 & 0 \end{bmatrix} \tag{2.57}$$

As shown in the Fig. (2.8) a general choice of fixed and moving reference planes transforms the coefficient matrix to the form below:

$$[Q'] = [C^{-1}]^T [Q][C^{-1}] \tag{2.58}$$

where, $[C] = [G^+][H^-]$ is the matrix form of the quaternion transformation to the new fixed and moving frames.

$$\begin{aligned} &[G] = (x/2, y/2, 0, 1), \\ &[H] = (h/2\cos(\alpha)/2, -h/2\sin(\alpha)/2, \sin(\alpha)/2, \cos(\alpha)/2) \end{aligned} \tag{2.59}$$

$$\mathbf{Z}'(\theta, \phi, b)[Q']\mathbf{Z}(\theta, \phi, b) \in [\frac{b_1 - a}{2}, \frac{b_2 + a}{2}] \tag{2.60}$$

Simplifying the above equation we get:

$$F(Z_1, Z_2, Z_3, Z_4) = (Z_1 - \sigma_1 Z_3 - \tau_1 Z_4)Z_4 + (Z_2 - \sigma_2 Z_3 - \tau_2 Z_4)Z_3, \text{and} \tag{2.61}$$

$$\begin{aligned} \sigma_1 &= (y + h\sin\alpha)/2, \qquad & \tau_1 &= (x + h\cos\alpha)/2, \\ \sigma_2 &= (-x + h\cos\alpha)/2, \qquad & \tau_2 &= (y - h\sin\alpha)/2. \end{aligned} \tag{2.62}$$

$$\frac{b_1 - a}{2} \leq F(Z_1, Z_2, Z_3, Z_4) \leq \frac{b_2 + a}{2}, \tag{2.63}$$

Eq.(2.63) characterize the kinematic constraints of a planar RRP open chain and define the constraint manifold for the chain.

Thus, the constraint manifold of the planar RRP closed chains is given by a pair of hyperbolic paraboloids and for the a mechanism to pass through a given motion, the image curve would have to be contained in the volume between the constraint manifolds.

Using the projective property of the planar quaternion, to visualize the hyper-geometric shape described by Eq.(2.63), we observe its intersection with the hyperplane $Z_4 = 1$; in the other words, we project Eq.(2.63) onto hyper-plane $Z_4 = 1$. Denote $(z_1, z_2, z_3, 1)$ as the projected point of (Z_1, Z_2, Z_3, Z_4), both of which represent the same planar displacement. Then, it is yielded that

$$F(z_1, z_2, z_3, 1) = (Z_1 - \sigma_1 Z_3 - \tau_1) + (Z_2 - \sigma_2 Z_3 - \tau_2) Z_3 \tag{2.64}$$

where σ_1, σ_2, τ_1 and τ_2 are the same as Eq.(2.62).

The volume field described by Eq.(2.64) creates implicit surfaces of (z_1, z_2, z_3). The means to develop the isosurface is to, without loss of generality, set $F(z_1, z_2, z_3, 1) = c$, $c \in [L_{\min}, L_{\max}]$, ($L_{\min} = \frac{b-a}{2}$ and $L_{\max} = \frac{2b+a}{2}$), and to be standard, we also reorganize Eq.(2.64);

$$Z_1 + (Z_2 - \sigma_2 Z_3 - \tau_2 - \sigma_1)Z_3 - \tau_1 = c \tag{2.65}$$

Reformulating the above equation we get the standard form as:

$$\sigma_2(Z_3^2 - \frac{Z_3}{\sigma_2}(Z_2 - (\tau_2 + \sigma_1))) = Z_1 - (\tau_1 + c) \tag{2.66}$$

This is a typical hyperbolic paraboloid in the projective (z_1, z_2, z_3) space. See Table (2.4). The saddle point of the hyperbolic paraboloid is located at $(\tau_1, \tau_2 + \sigma_1, 0)$. The central axis is $(1, 0, 0)$, so that the hyperbolic paraboloid orients along the $x-$ direction. It is evident to tell that the location of the saddle point and the mean curvature are decided by the location of the fixed pivot, the length of the floating link and the relative angle of $\mathbf{M}$ to the floating link. A representation of the pair of sheared hyperbolic paraboloids implemented in Mathematica are shown in Fig. (2.9).

As it can be referred from the parameters extracted from the standard equation of a hyperbolic paraboloid, it does not yield all the geometric parameters independently. Hence, in addition to the existing geometric parameters of location of the saddle point and the orientation, we need to define an addition geometric parameter. For a hyperbolic paraboloid the mean curvature of the surfaces at the saddle point yields σ_2. The mean curvature (H) is derived as follows:

$$H(u, v) = \frac{K_1(u, v) + K_2(u, v)}{2}, \tag{2.67}$$

where $K_1(u,v)$ and $K_2(u,v)$ are defined as principal curvatures of the surface at parameters (u,v). From the above Eq.(2.67), the differential form is;

$$H = \frac{1}{2}(\frac{EN - 2MF + GL}{EG - F^2}), \tag{2.68}$$

where E, F, G are the coefficients of the first fundamental form and L, M, N are the coefficients of the second fundamental form.

From the above differential Eq.(2.68), we get:

$$H = \sigma_2. \tag{2.69}$$

Table 2.4: Parameters for the projective sheared hyperbolic paraboloid presented by Eq.(2.66)

Geometric Features	Constraint Parameters
Saddle point	$(\tau_1, \tau_2 + \sigma_1, 0)$
Orientation	$(1, 0, 0)$
Mean curvature	σ_2
Distance between surfaces	$L_{min} \leq c \leq L_{max}$

2.4.3.1 Inverse Kinematics for Planar RRP Open Chain

The inverse kinematics problem is stated: Given the end-effector pose $\{X, Y, \delta\}^T$, calculate the three actuated joint (R or P) values [71]. In the case of an RRP open chain, the joint variables to be calculated are θ, b and ϕ. The notations used in the inverse kinematic relations are the same as used for the RRR open

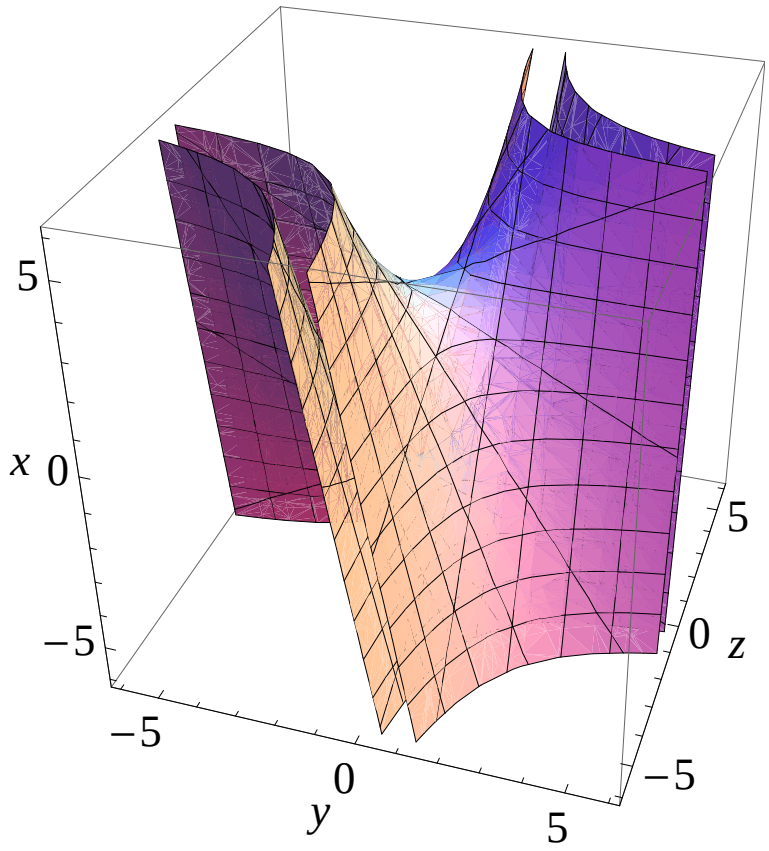

Figure 2.9: A pair of hyperbolic paraboloids representing a pair of constraint manifolds for a RRP open chain.

chain. The joint angles can be calculated using the following relations:

$$\theta = 2\tan^{-1}\left(\frac{-F \pm \sqrt{E^2 + F^2 - G^2}}{G - E}\right) \tag{2.70}$$

$$b = \frac{B_x - A_x - a\cos(\theta)}{\cos(\delta - \alpha)} \tag{2.71}$$

$$\phi = \delta - \alpha - \theta \tag{2.72}$$

Where, the values of E, F,and G are given by the following relations:

$$\begin{aligned} E &= a\sin(\delta - \alpha), \\ F &= -a\cos(\delta - \alpha), \\ G &= (B_x - A_y)\cos(\delta - \alpha) + A_x - B_x. \end{aligned} \tag{2.73}$$

2.4.4 Planar PRR Open Chain

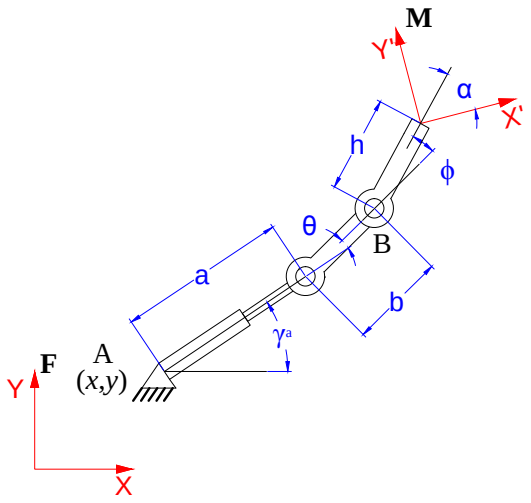

Figure 2.10: A planar PRR open chain

Consider a planar PRR open chain as shown in Fig. (2.10). The length of the first link is a, length of the second link is b and θ and ϕ are joint angles for two revolute joints respectively. In the figure, **F** and **M** mark the fixed and

the moving frames, respectively. The fixed pivot is located at (x, y), while the moving frame is located at a distance of h from the end revolute joint. The moving frame is assumed to be tilted by angle of α from the line joining the end pivot and the origin of the moving frame. When the fixed and moving frames are located at A and B respectively the parametrized equation of the constraint manifold $\mathbf{Z}(a, \theta, \phi)$ of a PRR open chain is obtained as follows:

$$\mathbf{Z}(a, \theta, \phi) = \mathbf{X}(a)\mathbf{Z}(\theta)\mathbf{X}(b)\mathbf{Z}(\phi). \tag{2.74}$$

The coordinates of $\mathbf{Z}(a, \theta, \phi) = (Z_1, Z_2, Z_3, Z_4)$ can be obtained as:

$$\begin{aligned} Z_1 &= a/2\cos(\theta+\phi)/2 + b/2\cos(\theta-\phi)/2, \\ Z_2 &= a/2\sin(\theta+\phi)/2 + b/2\sin(\theta-\phi)/2, \\ Z_3 &= \sin(\theta+\phi)/2, \\ Z_4 &= \cos(\theta+\phi)/2. \end{aligned} \tag{2.75}$$

From Eq.(2.75), it can be seen that the coordinates, Z_i, satisfy the following equations:

$$Z_1 Z_4 - Z_2 Z_3 = (a/2) + (b/2)\cos(\phi) \in [\tfrac{a_1-b}{2}, \tfrac{a_2+b}{2}] \tag{2.76}$$

$$Z_3^2 + Z_4^2 = 1. \tag{2.77}$$

From Eq.(2.76) we can see that the equation is very similar to that for

RRP configuration, also we get the quadratic form as:

$$\frac{a_1 - b}{2} \leq x^T[Q]x \leq \frac{a_1 + b}{2}. \tag{2.78}$$

with the coefficient matrix as:

$$Q = \begin{bmatrix} 0 & 0 & 0 & 1/2 \\ 0 & 0 & -1/2 & 0 \\ 0 & -1/2 & 0 & 0 \\ 1/2 & 0 & 0 & 0 \end{bmatrix} \tag{2.79}$$

As shown in the Fig. (2.10) a general choice of fixed and moving reference planes transforms the coefficient matrix to the form below:

$$[Q'] = [C^{-1}]^T[Q][C^{-1}] \tag{2.80}$$

where, $[C] = [G^+][H^-]$ is the matrix form of the quaternion transformation to the new fixed and moving frames.

$$[G] = (x/2, y/2, 0, 1), \tag{2.81}$$
$$[H] = (h/2\cos(\alpha)/2, -h/2\sin(\alpha)/2, \sin(\alpha)/2, \cos(\alpha)/2)$$

$$\mathbf{Z}'(a, \theta, \phi)[Q']\mathbf{Z}(a, \theta, \phi) \in [\frac{a_1 - b}{2}, \frac{a_2 + b}{2}] \tag{2.82}$$

Simplifying the above equation we get:

$$F(Z_1, Z_2, Z_3, Z_4) = (Z_1 - \sigma_1 Z_3 - \tau_1 Z_4)Z_4 - (Z_2 - \sigma_2 Z_3 - \tau_2 Z_4)Z_3, \text{and} \quad (2.83)$$

$$\begin{aligned} \sigma_1 &= (y + h\sin\alpha)/2, & \tau_1 &= (x + h\cos\alpha)/2, \\ \sigma_2 &= (-x + h\cos\alpha)/2, & \tau_2 &= (y - h\sin\alpha)/2. \end{aligned} \quad (2.84)$$

$$\frac{a_1 - b}{2} \leq F(Z_1, Z_2, Z_3, Z_4) \leq \frac{a_2 + b}{2}, \quad (2.85)$$

Eq.(2.85) characterize the kinematic constraints of a planar PRR open chain and define the constraint manifold for the chain.

Thus, the constraint manifold of the planar PRR closed chains is given by a pair of hyperbolic paraboloids and for the a mechanism to pass through a given motion, the image curve would have to be contained in the volume between the constraint manifolds.

Using the projective property of the planar quaternion, to visualize the hyper-geometric shape described by Eq.(2.85), we observe its intersection with the hyperplane $Z_4 = 1$; in the other words, we project Eq.(2.85) onto hyper-plane $Z_4 = 1$. Denote $(z_1, z_2, z_3, 1)$ as the projected point of (Z_1, Z_2, Z_3, Z_4), both of which represent the same planar displacement. Then, it is yielded that

$$F(z_1, z_2, z_3, 1) = (Z_1 - \sigma_1 Z_3 - \tau_1) - (Z_2 - \sigma_2 Z_3 - \tau_2)Z_3 \quad (2.86)$$

where σ_1, σ_2, τ_1 and τ_2 are the same as Eq.(2.84).

The volume field described by Eq.(2.86) creates implicit surfaces of (z_1, z_2, z_3). The means to develop the isosurface is to, without loss of generality, set $F(z_1, z_2, z_3, 1) = c$, $c \in [L_{\min}, L_{\max}]$, ($L_{\min} = \frac{a-b}{2}$ and $L_{\max} = \frac{2a+b}{2}$), and to be standard, we also reorganize Eq.(2.86);

$$Z_1 - (Z_2 - \sigma_2 Z_3 - \tau_2 - \sigma_1)Z_3 - \tau_1 = c \tag{2.87}$$

Reformulating the above equation we get the standard form as:

$$-\sigma_2(Z_3^2 - \frac{Z_3}{\sigma_2}(Z_2 - (\tau_2 - \sigma_1))) = Z_1 - (\tau_1 + c) \tag{2.88}$$

This is a typical hyperbolic paraboloid in the projective (z_1, z_2, z_3) space. See Table (2.5). The saddle point of the hyperbolic paraboloid is located at $(\tau_1, \tau_2 - \sigma_1, 0)$. The central axis is $(1, 0, 0)$, so that the hyperbolic paraboloid orients along the $x-$ direction. It is evident to tell that the location of the saddle point and the mean curvature are decided by the location of the fixed pivot, the length of the floating link and the relative angle of $\mathbf{M}$ to the floating link. A representation of the pair of sheared hyperbolic paraboloids implemented in Mathematica are shown in Fig. (2.11).

As it can be referred from the parameters extracted from the standard equation of a hyperbolic paraboloid, it does not yield all the geometric parameters independently. Hence, in addition to the existing geometric parameters of location of the saddle point and the orientation, we need to define an addi-

tion geometric parameter. For a hyperbolic paraboloid the mean curvature of the surfaces at the saddle point yields σ_2. The mean curvature (H) is derived using the equations (2.67 and 2.68), and we get

$$H = -\sigma_2. \tag{2.89}$$

Table 2.5: Parameters for the projective sheared hyperbolic paraboloid presented by Eq.(2.88)

Geometric Features	Constraint Parameters
Saddle point	$(\tau_1, \tau_2 - \sigma_1, 0)$
Orientation	$(1, 0, 0)$
Mean curvature	$-\sigma_2$
Distance between surfaces	$L_{min} \leq c \leq L_{max}$

2.4.4.1 Inverse Kinematics for Planar PRR Open Chain

The inverse kinematics problem is stated: Given the end-effector pose $\{X, Y, \delta\}^T$, calculate the three actuated joint (R or P) values [71]. In the case of an PRR open chain, the joint variables to be calculated are a, θ and ϕ. The notations used in the inverse kinematic relations are the same as used for the RRR open chain. The joint angles can be calculated using the following relations:

$$\theta = \sin^{-1}\left(\frac{B_y - A_y}{b}\right) \tag{2.90}$$

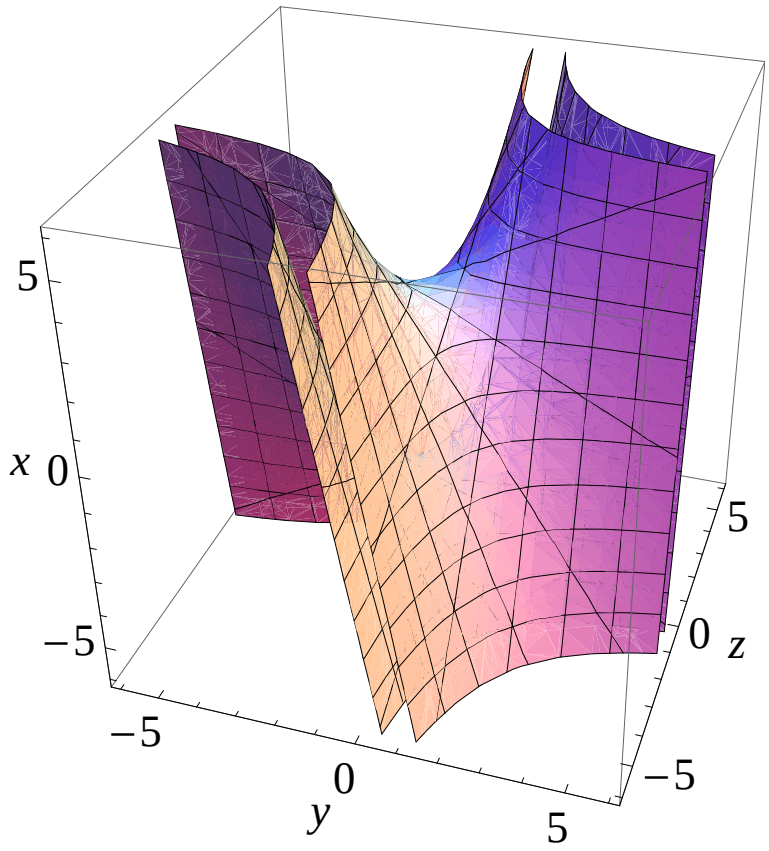

Figure 2.11: A pair of hyperbolic paraboloids representing a pair of constraint manifolds for a PRR open chain.

$$a = B_x - A_x - b\cos(\theta) \tag{2.91}$$

$$\phi = \delta - \alpha - \theta \tag{2.92}$$

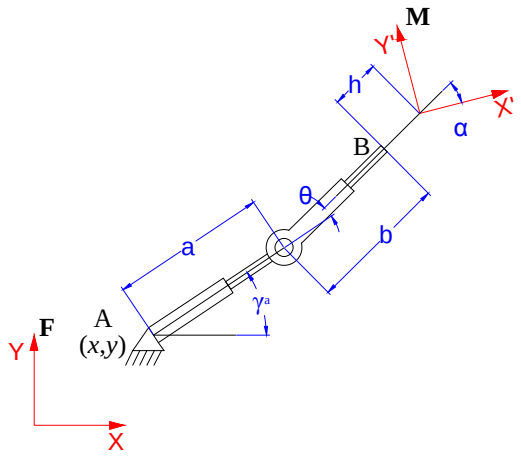

Figure 2.12: A planar PRP open chain

2.4.5 Planar PRP Open Chain

Consider a planar PRP open chain as shown in Fig. 2.12. The length of the first link is a, length of the second link is b and θ is the joint angle for the revolute joint. In the figure, **F** and **M** mark the fixed and the moving frames, respectively. The fixed pivot is located at (x, y), while the moving frame is located at a distance of h from the end of link b. The moving frame is assumed to be tilted by angle of α from the line joining the end pivot and the origin of the moving frame. When the fixed and moving frames are located at A and B respectively the parametrized equation of the constraint manifold $\mathbf{Z}(a, \theta, b)$ of a PRP open chain is obtained as follows:

$$\mathbf{Z}(a, \theta, b) = \mathbf{X}(a)\mathbf{Z}(\theta)\mathbf{X}(b). \tag{2.93}$$

The coordinates of $\mathbf{Z}(a,\theta,b) = (Z_1, Z_2, Z_3, Z_4)$ can be obtained as:

$$\begin{aligned} Z_1 &= (a+b)/2\cos(\theta)/2, \\ Z_2 &= (b-a)/2\sin(\theta)/2, \\ Z_3 &= \sin(\theta)/2, \\ Z_4 &= \cos(\theta)/2. \end{aligned} \tag{2.94}$$

From Eq.(2.94), it can be seen that the coordinates, Z_i, satisfy the following equations:

$$Z_1 Z_4 - Z_2 Z_3 = (a/2) - (b/2)\cos(\phi) \in [\tfrac{a_1-b_2}{2}, \tfrac{a_2+b_2}{2}] \tag{2.95}$$

$$Z_3^2 + Z_4^2 = 1. \tag{2.96}$$

From Eq.(2.95) we can see that the equation is very similar to that for RRP configuration, also we get the quadratic form as:

$$\frac{a_1 - b_2}{2} \leq x^T[Q]x \leq \frac{a_2 + b_2}{2}. \tag{2.97}$$

with the coefficient matrix as:

$$Q = \begin{bmatrix} 0 & 0 & 0 & 1/2 \\ 0 & 0 & -1/2 & 0 \\ 0 & -1/2 & 0 & 0 \\ 1/2 & 0 & 0 & 0 \end{bmatrix} \tag{2.98}$$

As shown in the Fig. (2.12) a general choice of fixed and moving reference planes transforms the coefficient matrix to the form below:

$$[Q'] = [C^{-1}]^T [Q][C^{-1}] \tag{2.99}$$

where, $[C] = [G^+][H^-]$ is the matrix form of the quaternion transformation to the new fixed and moving frames.

$$[G] = (x/2, y/2, 0, 1), \tag{2.100}$$
$$[H] = (h/2\cos(\alpha)/2, -h/2\sin(\alpha)/2, \sin(\alpha)/2, \cos(\alpha)/2)$$

$$\mathbf{Z}'(a, \theta, b)[Q']\mathbf{Z}(a, \theta, b) \in [\frac{a_1 - b_2}{2}, \frac{a_2 + b_2}{2}] \tag{2.101}$$

Simplifying the above equation we get:

$$F(Z_1, Z_2, Z_3, Z_4) = (Z_1 - \sigma_1 Z_3 - \tau_1 Z_4)Z_4 - (Z_2 - \sigma_2 Z_3 - \tau_2 Z_4)Z_3, \text{and} \tag{2.102}$$

$$\begin{aligned} \sigma_1 &= (y + h\sin\alpha)/2, \qquad & \tau_1 &= (x + h\cos\alpha)/2, \\ \sigma_2 &= (-x + h\cos\alpha)/2, \qquad & \tau_2 &= (y - h\sin\alpha)/2. \end{aligned} \tag{2.103}$$

$$\frac{a_1 - b_2}{2} \leq F(Z_1, Z_2, Z_3, Z_4) \leq \frac{a_2 + b_2}{2}, \tag{2.104}$$

Eq.(2.104) characterize the kinematic constraints of a planar PRP open chain and define the constraint manifold for the chain.

Thus, the constraint manifold of the planar PRP closed chains is given by a pair of hyperbolic paraboloids and for the a mechanism to pass through a given motion, the image curve would have to be contained in the volume between the constraint manifolds.

Using the projective property of the planar quaternion, to visualize the hyper-geometric shape described by Eq.(2.104), we observe its intersection with the hyperplane $Z_4 = 1$; in the other words, we project Eq.(2.104) onto hyperplane $Z_4 = 1$. Denote $(z_1, z_2, z_3, 1)$ as the projected point of (Z_1, Z_2, Z_3, Z_4), both of which represent the same planar displacement. Then, it is yielded that

$$F(z_1, z_2, z_3, 1) = (Z_1 - \sigma_1 Z_3 - \tau_1) - (Z_2 - \sigma_2 Z_3 - \tau_2) Z_3 \tag{2.105}$$

where σ_1, σ_2, τ_1 and τ_2 are the same as Eq.(2.103).

The volume field described by Eq.(2.105) creates implicit surfaces of (z_1, z_2, z_3). The means to develop the isosurface is to, without loss of generality, set

$F(z_1, z_2, z_3, 1) = c,\ c \in [L_{\min}, L_{\max}]$, ($L_{\min} = \frac{a-2b}{2}$ and $L_{\max} = \frac{2a+2b}{2}$), and to be standard, we also reorganize Eq.(2.105);

$$Z_1 - (Z_2 - \sigma_2 Z_3 - \tau_2 - \sigma_1)Z_3 - \tau_1 = c \tag{2.106}$$

Reformulating the above equation we get the standard form as:

$$-\sigma_2(Z_3^2 - \frac{Z_3}{\sigma_2}(Z_2 - (\tau_2 - \sigma_1))) = Z_1 - (\tau_1 + c) \tag{2.107}$$

This is a typical hyperbolic paraboloid in the projective (z_1, z_2, z_3) space. See Table (2.6). The saddle point of the hyperbolic paraboloid is located at $(\tau_1, \tau_2 - \sigma_1, 0)$. The central axis is $(1, 0, 0)$, so that the hyperbolic paraboloid orients along the $x-$ direction. It is evident to tell that the location of the saddle point and the mean curvature are decided by the location of the fixed pivot, the length of the floating link and the relative angle of $\mathbf{M}$ to the floating link. A representation of the pair of sheared hyperbolic paraboloids implemented in Mathematica are shown in Fig. (2.13).

As it can be referred from the parameters extracted from the standard equation of a hyperbolic paraboloid, it does not yield all the geometric parameters independently. Hence, in addition to the existing geometric parameters of location of the saddle point and the orientation, we need to define an addition geometric parameter. For a hyperbolic paraboloid the mean curvature of the surfaces at the saddle point yields σ_2. The mean curvature (H) is derived using the equations (2.67 and 2.68), and we get

$$H = -\sigma_2. \tag{2.108}$$

Table 2.6: Parameters for the projective sheared hyperbolic paraboloid presented by Eq.(2.107)

Geometric Features	Constraint Parameters
Saddle point	$(\tau_1, \tau_2 - \sigma_1, 0)$
Orientation	$(1, 0, 0)$
Mean curvature	$-\sigma_2$
Distance between surfaces	$L_{min} \leq c \leq L_{max}$

2.4.5.1 Inverse Kinematics for Planar PRP Open Chain

The inverse kinematics problem is stated: Given the end-effector pose $\{X, Y, \delta\}^T$, calculate the three actuated joint (R or P) values [71]. In the case of an PRP open chain, the joint variables to be calculated are θ, a and b. The notations used in the inverse kinematic relations are the same as used for the RRR open chain. The joint angles can be calculated using the following relations:

$$a = \frac{(B_x - A_x)\sin(\theta) - (B_y - A_y)\cos(\theta)}{\sin(\theta)} \tag{2.109}$$

$$b = \frac{(B_y - A_y)\cos(\theta)}{\sin(\theta)} \tag{2.110}$$

$$\theta = \delta - \alpha \tag{2.111}$$

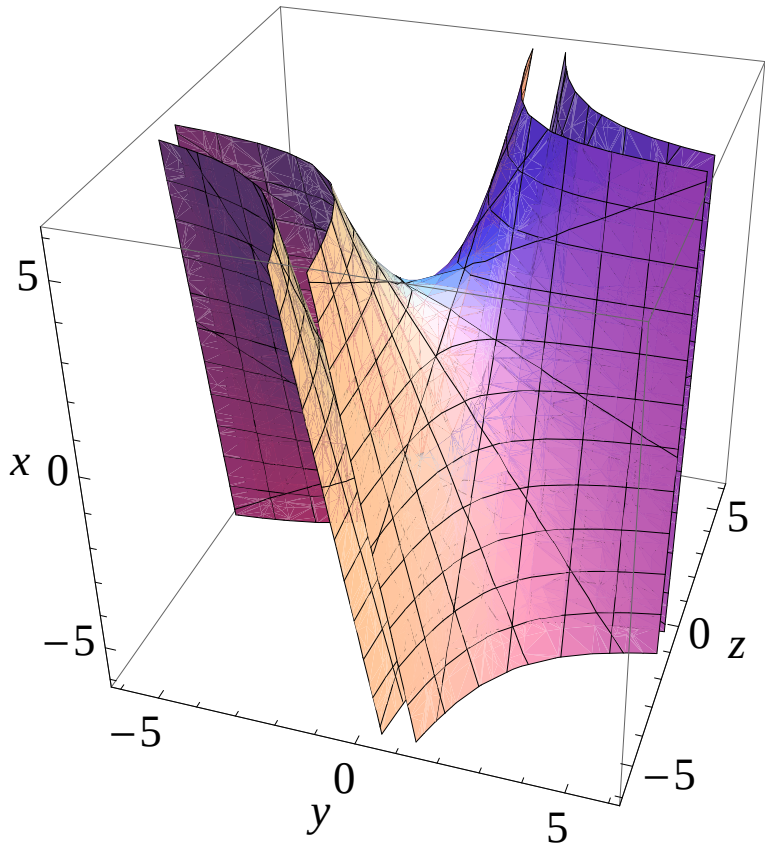

Figure 2.13: A pair of hyperbolic paraboloids representing a pair of constraint manifolds for a PRP open chain.

2.4.6 Planar PPR Open Chain

Consider a planar PPR open chain as shown in Fig. (2.14). The length of the first link is a, length of the second link is b, and their inclination angles are γ_a and γ_b respectively and θ is the joint angle for the revolute joint. In the figure, **F** and **M** mark the fixed and the moving frames, respectively. The fixed pivot is located at (x, y), while the moving frame is located at a distance of h from the end pivot. The moving frame is assumed to be tilted by angle of α from

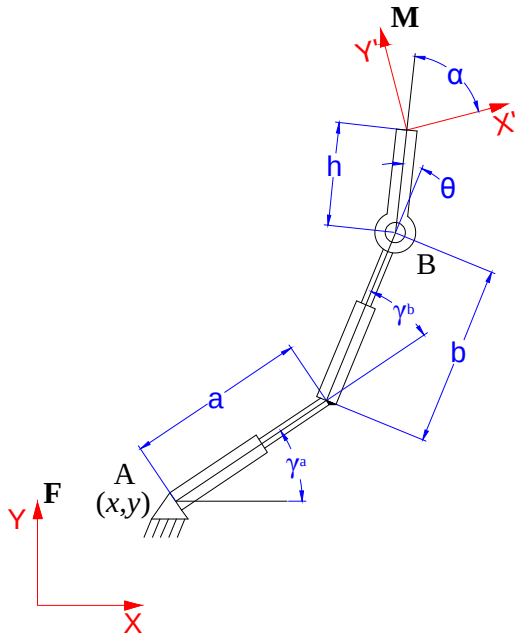

Figure 2.14: A planar PPR open chain

the line joining the end pivot and the origin of the moving frame. When the fixed and moving frames are located at A and B respectively the parametrized equation of the constraint manifold $\mathbf{Z}(a, b, \theta)$ of a PPR open chain is obtained as follows:

$$\mathbf{Z}(a, b, \theta) = \mathbf{Z}(\gamma_a)\mathbf{X}(a)\mathbf{Z}(\gamma_b)\mathbf{X}(b)\mathbf{Z}(\theta). \tag{2.112}$$

The coordinates of $\mathbf{Z}(a, b, \theta) = (Z_1, Z_2, Z_3, Z_4)$ can be obtained as:

$$\begin{aligned} Z_1 &= a/2\cos(\gamma_a - \gamma_b - \theta)/2 + b/2\cos(\gamma_a + \gamma_b - \theta)/2, \\ Z_2 &= a/2\sin(\gamma_a - \gamma_b - \theta)/2 + b/2\sin(\gamma_a + \gamma_b - \theta)/2, \end{aligned} \tag{2.113}$$

$$
\begin{aligned}
Z_3 &= \sin\left(\gamma_a + \gamma_b + \theta\right)/2, \\
Z_4 &= \cos\left(\gamma_a + \gamma_b + \theta\right)/2.
\end{aligned}
$$

From Eq.(2.113), it can be seen that the coordinates, Z_i, satisfy the following equations:

$$
Z_1 Z_4 - Z_2 Z_3 = (a/2)\cos(\gamma_a) - (b/2)\cos(\gamma_a + \gamma_b) \in [\tfrac{a_1\cos(\gamma_a)+b_1\cos(\gamma_a+\gamma_b)}{2}, \tfrac{a_2\cos(\gamma_a)+b_2\cos(\gamma_a+\gamma_b)}{2}] \tag{2.114}
$$

$$
Z_3^2 + Z_4^2 = 1. \tag{2.115}
$$

From Eq.(2.114) we can see that the equation is very similar to that for RRP configuration, also we get the quadratic form as:

$$
\frac{a_1\cos(\gamma_a) + b_1\cos(\gamma_a + \gamma_b)}{2} \leq x^T[Q]x \leq \frac{a_2\cos(\gamma_a) + b_2\cos(\gamma_a + \gamma_b)}{2}. \tag{2.116}
$$

with the coefficient matrix as:

$$
Q = \begin{bmatrix}
0 & 0 & 0 & 1/2 \\
0 & 0 & -1/2 & 0 \\
0 & -1/2 & 0 & 0 \\
1/2 & 0 & 0 & 0
\end{bmatrix} \tag{2.117}
$$

As shown in the Fig. (2.14) a general choice of fixed and moving reference planes transforms the coefficient matrix to the form below:

$$[Q'] = [C^{-1}]^T [Q][C^{-1}] \tag{2.118}$$

where, $[C] = [G^+][H^-]$ is the matrix form of the quaternion transformation to the new fixed and moving frames.

$$\begin{aligned} [G] &= (x/2, y/2, 0, 1), \\ [H] &= (h/2\cos(\alpha)/2, -h/2\sin(\alpha)/2, \sin(\alpha)/2, \cos(\alpha)/2) \end{aligned} \tag{2.119}$$

$$\mathbf{Z}'(a,b,\theta)[Q']\mathbf{Z}(a,b,\theta) \in [\frac{a_1\cos(\gamma_a) + b_1\cos(\gamma_a+\gamma_b)}{2}, \frac{a_2\cos(\gamma_a) + b_2\cos(\gamma_a+\gamma_b)}{2}] \tag{2.120}$$

Simplifying the above equation we get:

$$F(Z_1, Z_2, Z_3, Z_4) = (Z_1 - \sigma_1 Z_3 - \tau_1 Z_4)Z_4 - (Z_2 - \sigma_2 Z_3 - \tau_2 Z_4)Z_3, \text{and} \tag{2.121}$$

$$\begin{aligned} \sigma_1 &= (y + h\sin\alpha)/2, & \tau_1 &= (x + h\cos\alpha)/2, \\ \sigma_2 &= (-x + h\cos\alpha)/2, & \tau_2 &= (y - h\sin\alpha)/2. \end{aligned} \tag{2.122}$$

$$\frac{a_1\cos(\gamma_a)+b_1\cos(\gamma_a+\gamma_b)}{2} \leq F(Z_1,Z_2,Z_3,Z_4) \leq \frac{a_2\cos(\gamma_a)+b_2\cos(\gamma_a+\gamma_b)}{2}, \tag{2.123}$$

Eq.(2.123) characterize the kinematic constraints of a planar PPR open chain and define the constraint manifold for the chain.

Thus, the constraint manifold of the planar PPR closed chains is given by a pair of hyperbolic paraboloids and for the a mechanism to pass through a given motion, the image curve would have to be contained in the volume between the constraint manifolds.

Using the projective property of the planar quaternion, to visualize the hyper-geometric shape described by Eq.(2.123), we observe its intersection with the hyperplane $Z_4 = 1$; in the other words, we project Eq.(2.123) onto hyperplane $Z_4 = 1$. Denote $(z_1, z_2, z_3, 1)$ as the projected point of (Z_1, Z_2, Z_3, Z_4), both of which represent the same planar displacement. Then, it is yielded that

$$F(z_1,z_2,z_3,1) = (Z_1-\sigma_1 Z_3-\tau_1)-(Z_2-\sigma_2 Z_3-\tau_2)Z_3 \tag{2.124}$$

where σ_1, σ_2, τ_1 and τ_2 are the same as Eq.(2.122).

The volume field described by Eq.(2.124) creates implicit surfaces of (z_1, z_2, z_3). The means to develop the isosurface is to, without loss of generality, set $F(z_1, z_2, z_3, 1) = c$, $c \in [L_{\min}, L_{\max}]$, ($L_{\min} = \frac{a\cos(\gamma_a)+b\cos(\gamma_a+\gamma_b)}{2}$ and $L_{\max} = \frac{2a\cos(\gamma_a)+2b\cos(\gamma_a+\gamma_b)}{2}$), and to be standard, we also reorganize Eq.(2.124);

$$Z_1 - (Z_2 - \sigma_2 Z_3 - \tau_2 - \sigma_1)Z_3 - \tau_1 = c \tag{2.125}$$

Reformulating the above equation we get the standard form as:

$$-\sigma_2(Z_3^2 - \frac{Z_3}{\sigma_2}(Z_2 - (\tau_2 - \sigma_1))) = Z_1 - (\tau_1 + c) \tag{2.126}$$

This is a typical hyperbolic paraboloid in the projective (z_1, z_2, z_3) space. See Table (2.7). The saddle point of the hyperbolic paraboloid is located at $(\tau_1, \tau_2 - \sigma_1, 0)$. The central axis is $(1, 0, 0)$, so that the hyperbolic paraboloid orients along the $x-$ direction. It is evident to tell that the location of the saddle point and the mean curvature are decided by the location of the fixed pivot, the length of the floating link and the relative angle of $\mathbf{M}$ to the floating link. A representation of the pair of sheared hyperbolic paraboloids implemented in Mathematica are shown in Fig. (2.15).

As it can be referred from the parameters extracted from the standard equation of a hyperbolic paraboloid, it does not yield all the geometric parameters independently. Hence, in addition to the existing geometric parameters of center point (saddle point) and the orientation, we need to define an addition geometric parameter. For a hyperbolic paraboloid the mean curvature of the surfaces at the saddle point yields σ_2. The mean curvature (H) is derived using the equations (2.67 and 2.68), and we get

$$H = -\sigma_2. \tag{2.127}$$

Table 2.7: Parameters for the projective sheared hyperbolic paraboloid presented by Eq.(2.126)

Geometric Features	Constraint Parameters
Saddle point	$(\tau_1, \tau_2 - \sigma_1, 0)$
Orientation	$(1, 0, 0)$
Mean curvature	$-\sigma_2$
Distance between surfaces	$L_{min} \leq c \leq L_{max}$

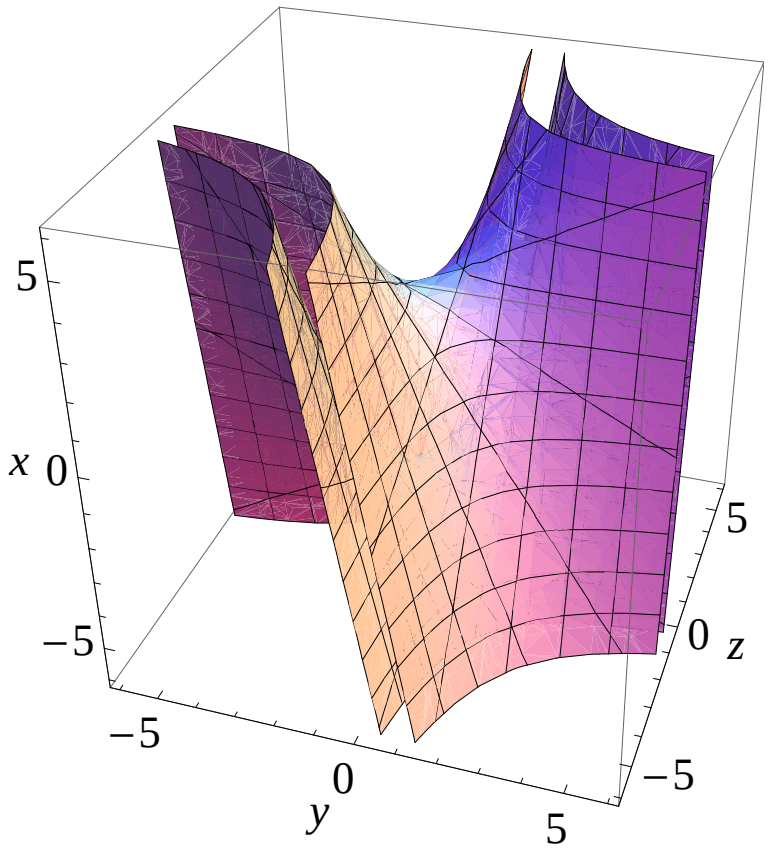

Figure 2.15: A pair of hyperbolic paraboloids representing a pair of constraint manifolds for a PPR open chain.

2.4.6.1 Inverse Kinematics for Planar PPR Open Chain

The inverse kinematics problem is stated: Given the end-effector pose $\{X, Y, \delta\}^T$, calculate the three actuated joint (R or P) values [71]. In the case of an PPR open chain, the joint variables to be calculated are θ, a and b. The notations used in the inverse kinematic relations are the same as used for the RRR open chain. The joint angles can be calculated using the following relations:

$$a = \frac{(B_x - A_x)\sin(\gamma_a + \gamma_b) - (B_y - A_y)\cos(\gamma_a + \gamma_b)}{\sin(\gamma_b)} \tag{2.128}$$

$$b = \frac{-(B_x - A_x)\sin(\gamma_a) + (B_y - A_y)\cos(\gamma_a)}{\sin(\gamma_b)} \tag{2.129}$$

$$\theta = \delta - \alpha \tag{2.130}$$

2.4.7 Planar RPP Open Chain

Consider a planar RPP open chain as shown in Fig. (2.16). The length of the first link is a, length of the second link is b, the inclination angle of the second link is γ_b and θ is the joint angle for the revolute joint. In the figure, **F** and **M** mark the fixed and the moving frames, respectively. The fixed pivot is located at (x, y), while the moving frame is located at a distance of h from the end of link b. The moving frame is assumed to be tilted by angle of α from the line joining the end pivot and the origin of the moving frame. When the fixed and moving frames are located at A and B respectively the parametrized

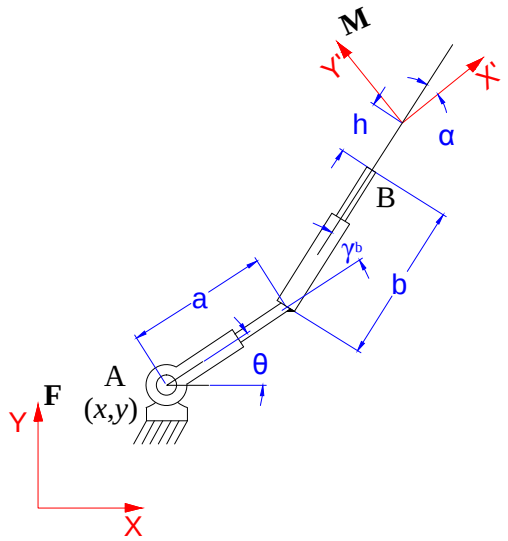

Figure 2.16: A planar RPP open chain

equation of the constraint manifold $\mathbf{Z}(\theta, a, b)$ of a RPP open chain is obtained as follows:

$$\mathbf{Z}(\theta, a, b) = \mathbf{Z}(\theta)\mathbf{X}(a)\mathbf{Z}(\gamma_b)\mathbf{X}(b). \tag{2.131}$$

The coordinates of $\mathbf{Z}(\theta, a, b) = (Z_1, Z_2, Z_3, Z_4)$ can be obtained as:

$$\begin{aligned} Z_1 &= a/2\cos(\theta - \gamma_b)/2 + b/2\cos(\theta + \gamma_b)/2, \\ Z_2 &= a/2\sin(\theta - \gamma_b)/2 + b/2\sin(\theta + \gamma_b)/2, \\ Z_3 &= \sin(\theta + \gamma_b)/2, \\ Z_4 &= \cos(\theta + \gamma_b)/2. \end{aligned} \tag{2.132}$$

From Eq.(2.132), it can be seen that the coordinates, Z_i, satisfy the following equations:

$$Z_1 Z_4 + Z_2 Z_3 = (a/2)\cos(\gamma_b) - (b/2) \in [\tfrac{a_1 \cos(\gamma_b)+b_1}{2}, \tfrac{a_2 \cos(\gamma_b)+b_2}{2}] \tag{2.133}$$

$$Z_3^2 + Z_4^2 = 1. \tag{2.134}$$

From Eq.(2.133) we can see that the equation is very similar to that for RRP configuration, also we get the quadratic form as:

$$\frac{a_1 \cos(\gamma_b) + b_1}{2} \leq x^T [Q] x \leq \frac{a_2 \cos(\gamma_b) + b_2}{2}. \tag{2.135}$$

with the coefficient matrix as:

$$Q = \begin{bmatrix} 0 & 0 & 0 & 1/2 \\ 0 & 0 & 1/2 & 0 \\ 0 & 1/2 & 0 & 0 \\ 1/2 & 0 & 0 & 0 \end{bmatrix} \tag{2.136}$$

As shown in the Fig. (2.16) a general choice of fixed and moving reference planes transforms the coefficient matrix to the form below:

$$[Q'] = [C^{-1}]^T [Q] [C^{-1}] \tag{2.137}$$

where, $[C] = [G^+][H^-]$ is the matrix form of the quaternion transformation to the new fixed and moving frames.

$$[G] = (x/2, y/2, 0, 1), \tag{2.138}$$
$$[H] = (h/2\cos(\alpha)/2, -h/2\sin(\alpha)/2, \sin(\alpha)/2, \cos(\alpha)/2)$$

$$\mathbf{Z}'(\theta, a, b)[Q']\mathbf{Z}(\theta, a, b) \in [\frac{a_1\cos(\gamma_b) + b_1}{2}, \frac{a_2\cos(\gamma_b) + b_2}{2}] \tag{2.139}$$

Simplifying the above equation we get:

$$F(Z_1, Z_2, Z_3, Z_4) = (Z_1 - \sigma_1 Z_3 - \tau_1 Z_4)Z_4 + (Z_2 - \sigma_2 Z_3 - \tau_2 Z_4)Z_3, \text{and} \tag{2.140}$$

$$\begin{aligned} \sigma_1 &= (y + h\sin\alpha)/2, & \tau_1 &= (x + h\cos\alpha)/2, \\ \sigma_2 &= (-x + h\cos\alpha)/2, & \tau_2 &= (y - h\sin\alpha)/2. \end{aligned} \tag{2.141}$$

$$\frac{a_1\cos(\gamma_b) + b_1}{2} \leq F(Z_1, Z_2, Z_3, Z_4) \leq \frac{a_2\cos(\gamma_b) + b_2}{2}, \tag{2.142}$$

Eq.(2.142) characterize the kinematic constraints of a planar RPP open chain and define the constraint manifold for the chain.

Thus, the constraint manifold of the planar RPP closed chains is given

by a pair of hyperbolic paraboloids and for the a mechanism to pass through a given motion, the image curve would have to be contained in the volume between the constraint manifolds.

Using the projective property of the planar quaternion, to visualize the hyper-geometric shape described by Eq.(2.142), we observe its intersection with the hyperplane $Z_4 = 1$; in the other words, we project Eq.(2.142) onto hyperplane $Z_4 = 1$. Denote $(z_1, z_2, z_3, 1)$ as the projected point of (Z_1, Z_2, Z_3, Z_4), both of which represent the same planar displacement. Then, it is yielded that

$$F(z_1, z_2, z_3, 1) = (Z_1 - \sigma_1 Z_3 - \tau_1) + (Z_2 - \sigma_2 Z_3 - \tau_2) Z_3 \tag{2.143}$$

where σ_1, σ_2, τ_1 and τ_2 are the same as Eq.(2.141).

The volume field described by Eq.(2.143) creates implicit surfaces of (z_1, z_2, z_3). The means to develop the isosurface is to, without loss of generality, set $F(z_1, z_2, z_3, 1) = c$, $c \in [L_{\min}, L_{\max}]$, ($L_{\min} = \frac{a\cos(\gamma_b)+b}{2}$ and $L_{\max} = \frac{2a\cos(\gamma_b)+2b}{2}$), and to be standard, we also reorganize Eq.(2.143);

$$Z_1 + (Z_2 - \sigma_2 Z_3 - \tau_2 - \sigma_1) - \tau_1 = c \tag{2.144}$$

Reformulating the above equation we get the standard form as:

$$\sigma_2 (Z_3^2 - \frac{Z_3}{\sigma_2}(Z_2 - (\tau_2 + \sigma_1))) = Z_1 - (\tau_1 + c) \tag{2.145}$$

This is a typical hyperbolic paraboloid in the projective (z_1, z_2, z_3) space.

See Table (2.8). The saddle point of the hyperbolic paraboloid is located at $(\tau_1, \tau_2 + \sigma_1, 0)$. The central axis is $(1, 0, 0)$, so that the hyperbolic paraboloid orients along the $x-$ direction. It is evident to tell that the location of the saddle point and the mean curvature are decided by the location of the fixed pivot, the length of the floating link and the relative angle of $\mathbf{M}$ to the floating link. A representation of the pair of sheared hyperbolic paraboloids implemented in Mathematica are shown in Fig. (2.17).

As it can be referred from the parameters extracted from the standard equation of a hyperbolic paraboloid, it does not yield all the geometric parameters independently. Hence, in addition to the existing geometric parameters of center point (saddle point) and the orientation, we need to define an addition geometric parameter. For a hyperbolic paraboloid the mean curvature of the surfaces at the saddle point yields σ_2. The mean curvature (H) is derived using the equations (2.67 and 2.68), and we get

$$H = \sigma_2. \tag{2.146}$$

Table 2.8: Parameters for the projective sheared hyperbolic paraboloid presented by Eq.(2.145)

Geometric Features	Constraint Parameters
Saddle point	$(\tau_1, \tau_2 + \sigma_1, 0)$
Orientation	$(1, 0, 0)$
Mean curvature	σ_2
Distance between surfaces	$L_{min} \leq c \leq L_{max}$

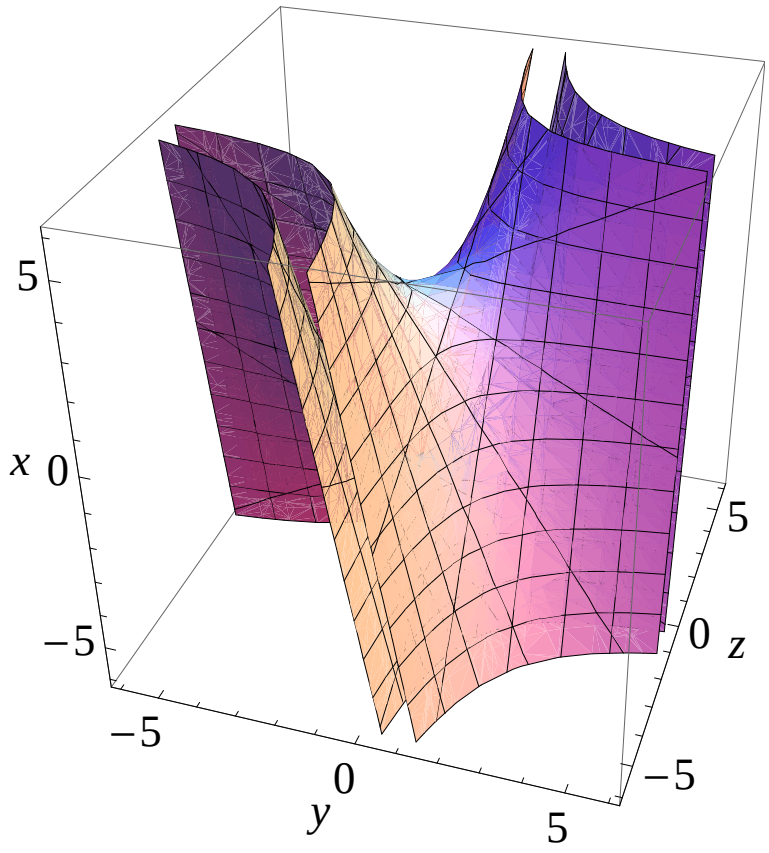

Figure 2.17: A pair of hyperbolic paraboloids representing a pair of constraint manifolds for a RPP open chain.

2.4.7.1 Inverse Kinematics for Planar RPP Open Chain

The inverse kinematics problem is stated: Given the end-effector pose $\{X, Y, \delta\}^T$, calculate the three actuated joint (R or P) values [71]. In the case of an RPP open chain, the joint variables to be calculated are θ, a and b. The notations used in the inverse kinematic relations are the same as used for the RRR open chain. The joint angles can be calculated using the following relations:

$$a = \frac{(B_x - A_x)\sin(\gamma_a + \gamma_b) - (B_y - A_y)\cos(\gamma_a + \gamma_b)}{\sin(\gamma_b)} \tag{2.147}$$

$$b = \frac{-(B_x - A_x)\sin(\gamma_a) + (B_y - A_y)\cos(\gamma_a)}{\sin(\gamma_b)} \tag{2.148}$$

$$\theta = \delta - \alpha \tag{2.149}$$

Summarizing all the above kinematic constraint equations and the respective constraint manifolds. The constraint manifold for a planar parallel manipulator is the common volume between all the three pairs of surfaces. When the image curve lies inside this common volume, a planar parallel manipulator is designed. A figure portraying the constraint manifold for a planar parallel manipulator is shown below.

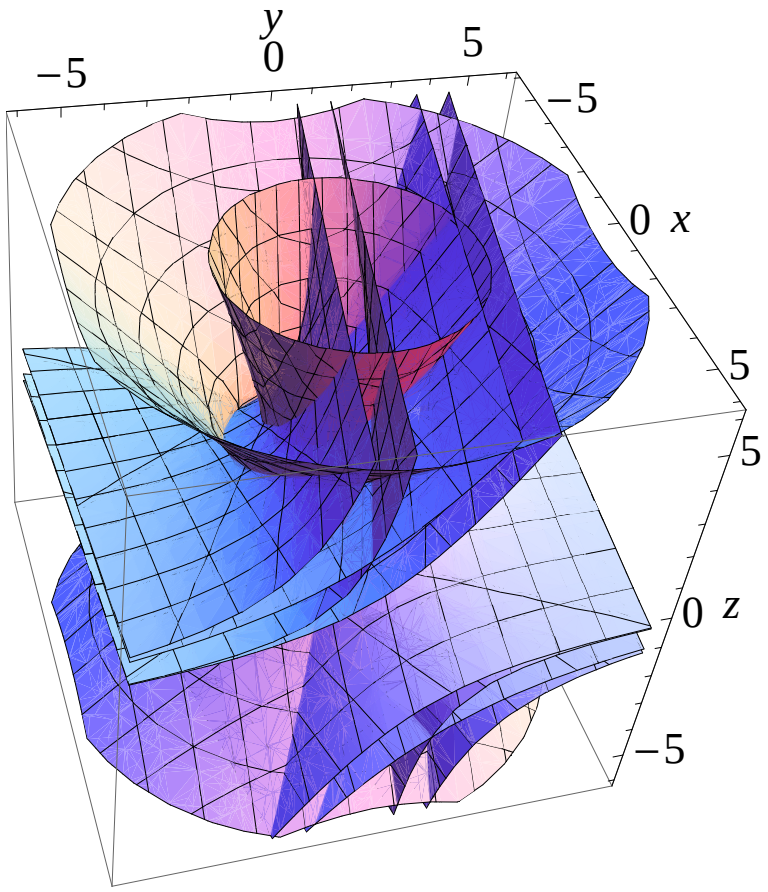

Figure 2.18: A constraint manifold for a planar parallel manipulator with RRR, RRP, and RPP Open Chains.

Chapter 3

Interactive Dimensional Synthesis and Motion Design

3.1 Interactive Dimensional Synthesis

The design method treats a three legged planar parallel manipulator as three independent 3-DOF open chains assembled together at the end. The constraint manifold of all the chains are geometric objects in the image space, the size, shape and position of which are a function of the mechanism parameters. A given rational motion maps to an image curve that needs to be contained inside the volume between these constraint manifolds. This section, describes the procedure required to design a planar parallel manipulator. It also describes the user interface with which the designer needs to be familiar with. The basic idea is that the designers are provided with a set of controls via the graphical

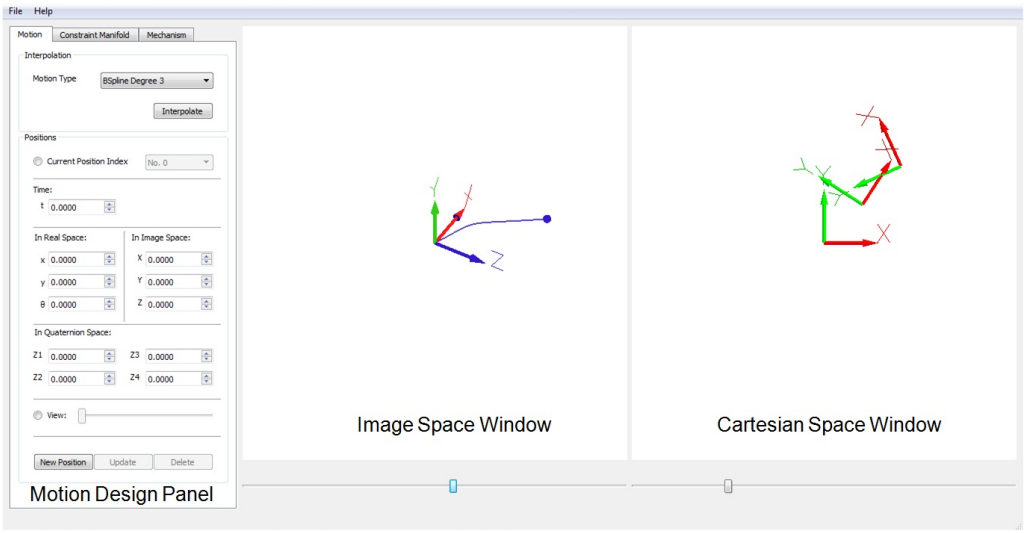

Figure 3.1: A screenshot of the motion design panel and the window spaces

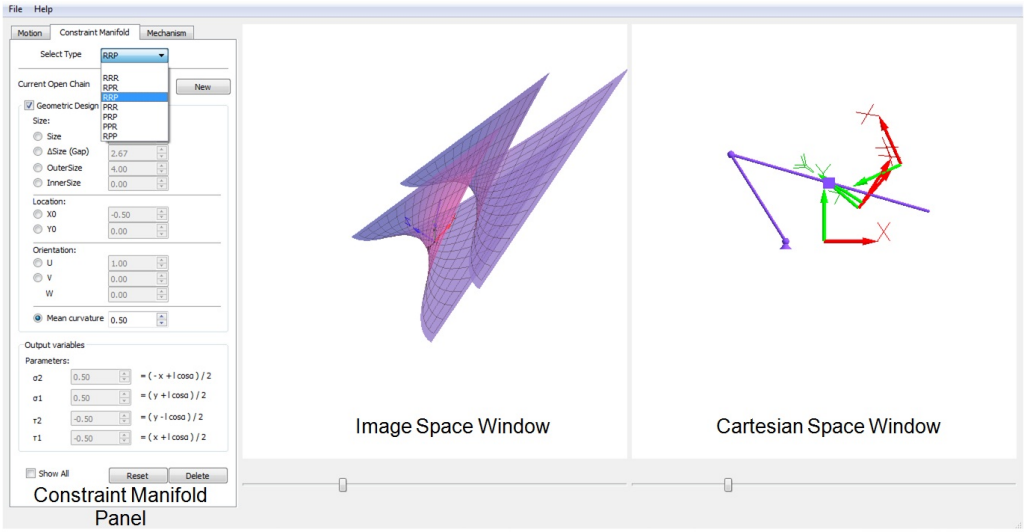

Figure 3.2: A screenshot of the manifold design panel and the window spaces

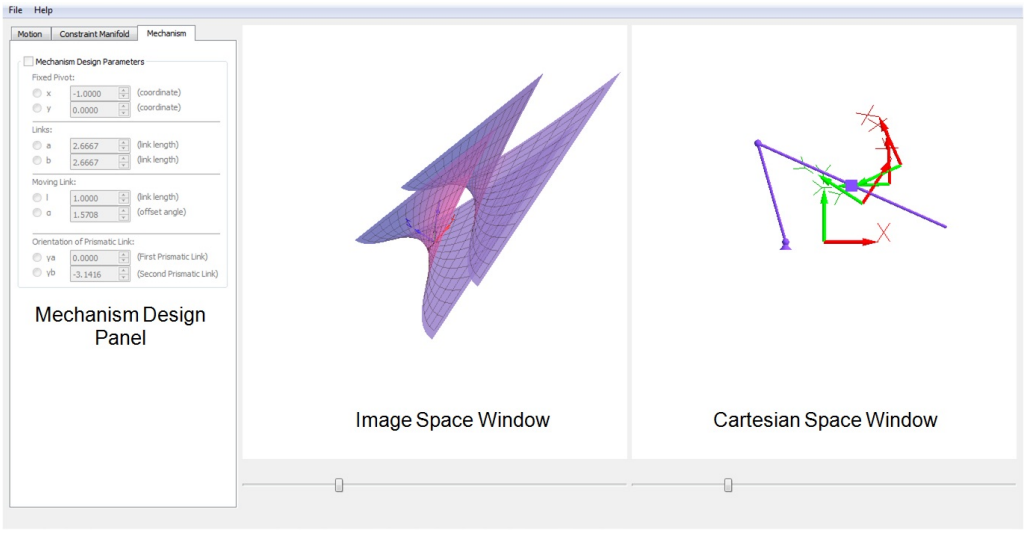

Figure 3.3: A screenshot of the mechanism design panel and the window spaces

user interface (GUI) of the tool that will allow them to interactively manipulate the constraint manifold with the objective to contain the image curve in volume between the pair of constraint manifold. Upon being satisfied visually, the designer will be allowed to instruct the program to check if there are any violations of the kinematic constraints. A windows binary of the tool for x86 architecture can be downloaded at `http://cadcam.eng.sunysb.edu/software`.

3.1.1 User Interface Functionalities

In terms of functionalities, the GUI has five parts, as shown in Figs. (3.1), (3.2), and (3.3).

1. The Cartesian Space Window (CSW): This window is used to display the given positions, the animation of the mechanism and the open chains

in the Cartesian space.

2. The Image Space Window (ISW): In this window, the constraint manifold as well as the image curve projected on the hyperplane are shown.

3. Motion Design Panel (MoDP): This panel supports operations like position insertion, deletion and modification, and comprises of functions to animate the motion and to test for constraint violation. The constraint violation test is done and the test results are visualized through the user interface. This operation updates both the Cartesian Space Window and the Image space Window.

4. Constraint Manifold Panel (CoMP): There are two ways to edit the mechanism: 1) directly manipulate mechanism parameters in the Cartesian space, like the location, the link lengths and the relative angle, and as a consequence, constraint manifolds change in the image space, or 2) Edit the geometric parameters that change the size, position, and the orientation of the manifolds.

   This panel allows the user to manipulate the geometric parameters associated with the constraint manifold so as to contain the image curve.This approach is more intuitive.

5. Mechanism Design Panel (MeDP): This panel allows the user to manipulate the mechanism parameters such as location of fixed pivot, link lengths, and relative angles associated with the open chain.

3.2 Design Procedure

1. Use the Motion Design panel to input given positions, associated time parameter, and interpolate them using a NURBS motion.

   The given planar positions can be input with the time parameter t, either using planar quaternion coordinates (Z_1, Z_2, Z_3, Z_4), or Cartesian coordinate directly (x, y, δ). Once all given positions are input, a cubic C^2 B-Spline motion that interpolates the given positions is generated. Consequently, the ISW shows the image points of the prescribed positions, and renders a continuous NURBS curve which passes through all the image points; while the CSW shows the given positions and the rational motion.

2. Switch to the Constraint Manifold panel. Dimensional synthesis starts with the choice of RRR, RPR, RRP, PRR, PRP, PPR, RPP open chains. The procedure for all the chains is very similar, hence only one open chain is discussed below, exceptions are described:

   In the CSW, initially, the fixed pivots are located at $(x_1, y_1) = (0, 0)$; the three links have unit length $a_1 = b_1 = h_1 = 1$, and the relative angle of $\mathbf{M}$ to the floating link is $\alpha_1 = 0$. In the ISW, a pair of surfaces appear (For RRR and RPR the surface is a hyperboloid, for the rest it is a hyperbolic paraboloid). The default surface pair will be visualized initially. At this point, it will be apparent that the image curve is not completely contained between the pair of surfaces, which means that the

constraints are being violated.

3. Modify the constraint manifold visually (for cases PPR and RPP set the orientation of the prismatic joints from MeDP initially, then modify constraint manifold) using the spinner controls (up and down arrows next to parameters) provided in the CoMP until the curve seems completely contained between the two pairs of surfaces. Dragging the slider in either ISW or CSW verifies if the constraints are actually satisfied or not. Using the current value of the mechanism parameters, the program automatically checks the constraint equations if they are satisfied. When they are satisfied, the program outputs links' length, fixed and moving pivot locations, and the orientation of the moving frame.

4. Repeat steps 2, 3 and 4, and synthesize the other two open chain.

5. Also note there can be several combinations to have a three legged planar parallel manipulator. Each leg can be chosen from the given configurations, *RRR, RPR, RRP, PRR, PRP, PPR, RPP.*

3.3 Example 1 for Planar Parallel Manipulator

In this section, an example is shown that demonstrates the dimensional synthesis of a planar parallel manipulator (RRR, RPR and RRP) using the constraint manifold modification for a given degree six rational motion.

Table 3.1: Cartesian coordinates of four prescribed positions along with their time parameter values

i	x,	y,	$\delta(^\circ)$	u_i
0	0.0448	0.1940	0	0.0
1	1.2067	1.5029	30	0.3
2	2.894	1.4852	15	0.6
3	2.045	2.8478	9	1.0

In this example, we use four positions as given in Table 3.1. The positions are given in Cartesian coordinate (x, y, δ), which specify the location of origin of moving frame $\mathbf{M}$ and the relative angle of $\mathbf{M}$ to horizontal axis of the fixed frame. Also given are the time parameter values (u_i) associated with each position. First, the given positions are converted to planar quaternion representation (Z_1, Z_2, Z_3, Z_4) and then they are interpolated using a degree six NURBS motion. The image curve is visualized using Rodrigues parameters (see Bottema and Roth [6]) given by $(Z_1/Z_4, Z_2/Z_4, Z_3/Z_4)$. Hereafter, one RRR open chains called A, one RPR open chain called B and one RRP open chain called C and their constraint manifolds are initialized. However, navigating through the motion, it is found that the constraints are violated – this shows up as the image curve being outside the manifold. The designer next modifies the constraint manifolds by varying various geometric parameters interactively. Different parameters have different effect on the size, position, and orientation of the manifold and the process is intuitive. Once the synthesis of three individual open chains A,B and C is completed (see Figs.(3.4), (3.5)

and (3.6)), the assembly of A, B and C yields a planar parallel manipulator (see Fig. 3.7) that passes through the given four positions with a continuous motion. Table 3.2 lists the design results.

Table 3.2: Synthesis parameters planar parallel manipulator, example 1

	x_1	y_1	a_1	b_1	h_1	α_1
Open Chain A (RRR)	0.5	3.0	4.5	2.5	3.354	-1.107
	x_2	y_2	b_1	b_2	h_2	α_2
Open Chain B (RPR)	2.0	0.0	3.5	2.5	3.0	0.0
	x_3	y_3	a_3	b_3	h_3	α_3
Open Chain C(RRP)	-1.5	0.0	2.67	2.67	1.118	2.034

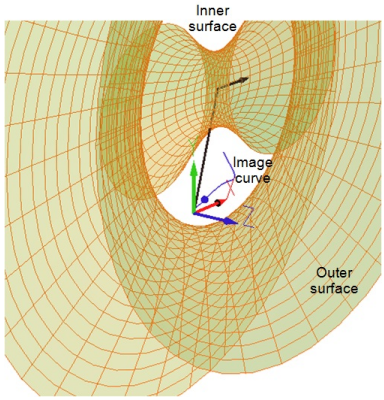

Figure 3.4: Constraint manifold of the RRR Open Chain A and image curve; in this figure, the image curve is completely contained inside the manifold.

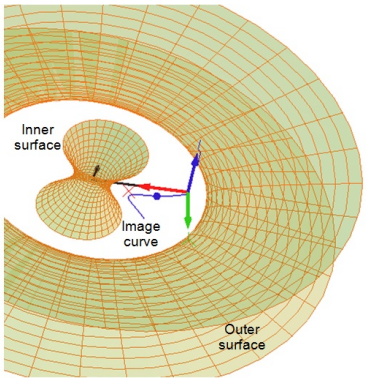

Figure 3.5: Constraint manifold of the RPR Open Chain B and image curve; in this figure, the image curve is completely contained inside the manifold.

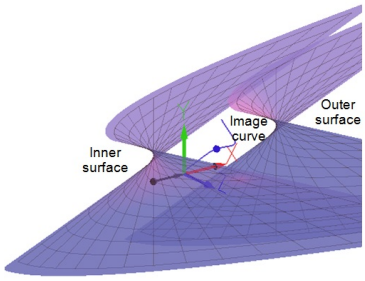

Figure 3.6: Constraint manifold of the RRP Open Chain C and image curve; in this figure, the image curve is completely contained inside the manifold.

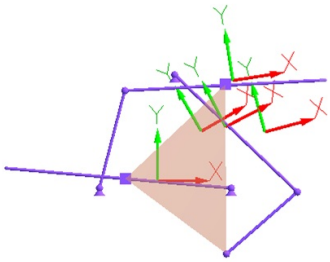

Figure 3.7: Planar parallel manipulator consisting of RRR, RPR, and RRP type legs.

3.4 Example 2 for Planar Parallel Manipulator

In this section, an example is shown that demonstrates the dimensional synthesis of a planar parallel manipulator (PRR, PRP and PPR) using the constraint manifold modification for a given degree six rational motion. In this example, for all the chains the inclination of the first 'P' joint is considered to be $0\,^{\circ}$, and for chain PPR the inclination of the second 'P' joint with respect to the first 'P' joint is considered to be $30\,^{\circ}$.

Table 3.3: Cartesian coordinates of four prescribed positions along with their time parameter values

i	x,	y,	$\delta(^{\circ})$	u_i
0	0.0448	0.1940	0	0.0
1	1.2067	1.5029	30	0.3
2	2.894	1.4852	15	0.6
3	2.045	2.8478	9	1.0

In this example, we use four positions as given in Table 3.3. The positions are given in Cartesian coordinate (x, y, δ), which specify the location of origin of moving frame $\mathbf{M}$ and the relative angle of $\mathbf{M}$ to horizontal axis of the fixed frame. Also given are the time parameter values (u_i) associated with each position. Hereafter, one PRR open chains called D, one PRP open chain called E and one PPR open chain called F and their constraint manifolds are initialized. However, navigating through the motion, it is found that the

constraints are violated – this shows up as the image curve being outside the manifold. The designer next modifies the constraint manifolds by varying various geometric parameters interactively. Different parameters have different effect on the size, position, and orientation of the manifold and the process is intuitive. Once the synthesis of three individual open chains D, E and F is completed (see Figs. (3.8), (3.9) and (3.10)), the assembly of D, E and F yields a planar parallel manipulator that passes through the given four positions with a continuous motion. Table 3.4 lists the design results.

Table 3.4: Synthesis parameters planar parallel manipulator, example 2

	x_1	y_1	a_1	b_1	h_1	α_1
Open Chain D (PRR)	-2.0	3.0	3.33	3.33	1.0	3.1416
	x_2	y_2	a_2	b_2	h_2	α_2
Open Chain E (PRP)	-2.0	1.0	4.0	1.0	3.0	3.1416
	x_3	y_3	a_3	b_3	h_3	α_3
Open Chain F (PPR)	-4.0	0.0	3.75	3.75	3.0	3.1416

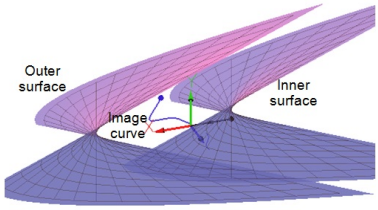

Figure 3.8: Constraint manifold of the PRR Open Chain D and image curve; in this figure, the image curve is completely contained inside the manifold.

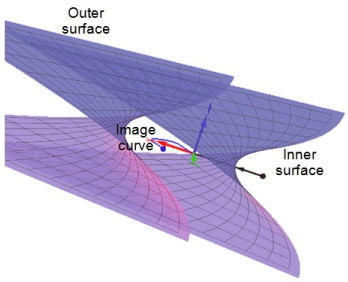

Figure 3.9: Constraint manifold of the PRP Open Chain E and image curve; in this figure, the image curve is completely contained inside the manifold.

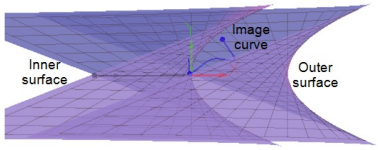

Figure 3.10: Constraint manifold of the PPR Open Chain F and image curve; in this figure, the image curve is completely contained inside the manifold.

Chapter 4

Conclusion

Planar parallel manipulator's have been successfully studied and implemented and their kinematic constraints have been discussed. Chapter 3 shows the implementation of these types of mechanism's. With the current approach the user is provided with the facility to design motions and mechanisms as well as for trajectory verification.

1. For designing of motion and mechanisms, a detailed procedure has been discussed in Chapter 3.

2. For the purposes of trajectory verification. The user can quickly verify whether the available mechanism will be able to perform the required task, by inputting the various mechanism parameters and verifying if the geometric constrains are being violated.

Although the research implemented will serve as a good tool for designers and for further researchers, it faces some limitations in its functionality and usage.

The current approach undertaken does not account for the singularity spaces associated with the mechanisms. This area can be further researched on, and the approach can be modified to account for these singularity spaces.

I see my work as an extension to the 6R planar closed chain and the RRR and RPR planar parallel manipulator software. There is a lot of scope for the expansion of this software to account for the singularities faced by the mechanisms, providing enhanced features for trajectory verification, selection of best suited chain for a given motion, and providing optimized mechanism parameters.

It is hoped that this software aids researchers, students, professors as well as other professionals working in CAGD, Computational Kinematics, Motion Design and other related fields.

Bibliography

[1] Merlet, J. P., 2006. Parallel Robots. Springer.

[2] Blaschke, W., 1911. "Euklidische kinematik und nichteuklidische geometrie". *Zeitschr. Math. Phys.,* **60**, pp. 61–91 and 203–204.

[3] Grunwald, J., 1911. "Ein abbildungsprinzip, welches die ebene geometrie und kinematik mit der raumlichen geometrie verknupft". *Sitzber. Ak. Wiss. Wien,* **120**, pp. 677–741.

[4] Ravani, B., and Roth, B., 1983. "Motion synthesis using kinematic mappings". *Journal of Mechanisms Transmissions and Automation in Design-Transactions of the Asme,* **105**(3), pp. 460–467.

[5] Ravani, B., and Roth, B., 1984. "Mappings of spatial kinematics". *Journal of Mechanisms Transmissions and Automation in Design-Transactions of the ASME,* **106**(3), pp. 341–347.

[6] Bottema, O., and Roth, B., 1979. *Theoretical Kinematics*. North Holland, Amsterdam.

[7] McCarthy, J. M., 1990. *Introduction to Theoretical Kinematics.* MIT, Cambridge, Mass.

[8] Ge, Q. J., and Ravani, B., 1994. "Computer-aided geometric design of motion interpolants". *ASME Journal of Mechanical Design,* **116**(3), pp. 756–762.

[9] Ge, Q. J., and Ravani, B., 1994. "Geometric construction of bezier motions". *ASME Journal of Mechanical Design,* **116**(3), pp. 749–755.

[10] Juttler, B., and Wagner, M. G., 1996. "Computer-aided design with spatial rational b-spline motions". *ASME Journal of Mechanical Design,* **118**(2), pp. 193–201.

[11] Wagner, M. G., 1994. "A geometric approach to motion design". Ph.d. dissertation.

[12] Röschel, O., 1998. "Rational motion design - a survey". *Computer-Aided Design,* **30**(3), pp. 169–178.

[13] Purwar, A., Chi, X., and Ge, Q. J., 2008. "Automatic fairing of two-parameter rational b-spline motion". *ASME Journal of Mechanical Design,* **130**(1), p. 011003.

[14] Purwar, A., and Ge, Q. J., 2005. "On the effect of dual weights in computer aided design of rational motions". *ASME Journal of Mechanical Design,* **127**(5), pp. 967–972.

[15] Bodduluri, R. M. C., and McCarthy, J. M., 1992. "Finite position synthesis using image curve of a spherical four-bar motion". *ASME J. of Mechanical Design,* **114**(1).

[16] Bodduluri, R., 1990. "Design and planned movement of multi-degree of freedom spatial mechanisms". Ph.d. dissertation.

[17] Larochelle, P., 1994. "Design of cooperating robots and spatial mechanisms". Phd dissertation.

[18] Hayes, M. J. D., Luu, T., and Chang, X.-W., 2004. *Kinematic Mapping Application to Approximate Type and Dimension Synthesis of Planar Mechanisms.* 9th Advances in Robotic Kinematics. Kluwer Academic Publishers, Dordrecht, The Netherlands.

[19] Brunnthaler, K., Schrocker, H., and Husty, M., 2006. *Synthesis of spherical four-bar mechanisms using spherical kinematic mapping.* Advances in Robot Kinematics. Springer, Netherlands.

[20] Venkataramanujam, V., and Larochelle, P., 2007. "Approximate motion synthesis of spherical kinematic chains". In Proceedings of ASME 2007 International Design Engineering Technical Conferences & Computers and Information in Engineering, Paper No. DETC2007-34372.

[21] Hayes, M. J. D., and Husty, M., 2003. "On the kinematic constraint surfaces of general three-legged planar robot platforms". Mechanism and Machine Theory, **38**(379394).

[22] Hayes, M., 1999. "Kinematics of general planar stewart-gough platforms". Ph.d. dissertation.

[23] Hayes, M. J. D., Zsombor-Murray, P. J., and Chen, C., 2004. "Kinematic analysis of general planar parallel manipulators". ASME J. of Mechanical Design, **126**(5).

[24] Murray, A. P., Pierrot, F., Dauchez, P., and McCarthy, J. M., 1997. "A planar quaternion approach to the kinematic synthesis of a parallel manipulator". Robotica, **15**, pp. 361-365. Article Part 4.

[25] Wu, J., Purwar, A., and Ge, Q. J., 2010, "Interactive Dimensional Synthesis and Motion Design of Planar 6R Single-Loop Closed Chains via Constraint Manifold Modification". *ASME Journal of Mechanisms and Robotics,* **2**, pp. 31012(8 pages)

[26] Purwar, A., Wu, J., Gupta, A., Ge, Q.J., 2010, "A Visual, Interactive Approach to Synthesis of Spherical 6R Closed Chains for Rational Motions via Constraint Manifold Modification". In 2010 ASME Mechanisms and Robotics Conference, Montreal, Canada, August 15-18, Paper No. DETC2010-28874.

[27] RUBEL, A. J., and KAUFMAN, R. E., 1977. "Kinsyn III: A new human-engineered system for interactive computer-aided design of planar linkages". *ASME Journal of Engineering for Industry,* **99**, p. 440448.

[28] Erdman, A., and Gustafson, J., 1977. Lincages: Linkage interactive computer analysis and graphically enhanced synthesis packages,. Tech. rep.

[29] Erdman, A. G., and Riley, D., 1981. "Computer-aided linkage design using the lincages package". In ASME Design Engineering Technical Conferences, ASME Press. Paper Number 81-DET-121.

[30] Kihonge, J., Vance, J., and Larochelle, P., 2001. "Spatial mechanism design in virtual reality with networking". In ASME 2001 Design Engineering Technical Conferences.

[31] Larochelle, P. M., 1998. "Spades: Software for synthesizing spatial 4C linkages". In ASME Design Engineering Technical Conferences (DETC).

[32] Larochelle, P. M., Dooley, A. P., Murray, A. P., and McCarthy, J. M., 1993. "Sphinx: Software for synthesizing spherical 4R mechanisms". In NSF Design and Manufacturing Systems Conference, pp. 607-611.

[33] Ruth, D., and McCarthy, J. M., 1997. "Sphinxpc: An implementation of four position synthesis for planar and spherical 4R linkages". In ASME Design Engineering Technical Conferences (DETC).

[34] Tse, D., and Larochelle, P. M., 1999. "Osiris: a new generation spherical and spatial mechanism cad program". In 1999 Florida Conference on Recent Advancements in Robotics.

[35] Perez, A., and McCarthy, J., 2000. "Dimensional synthesis of spatial RR robots". In Advances in Robot Kinematics.

[36] Su, H., and McCarthy, J. M., 2001. "Classification of designs for RRSS linkages". In ASME Design Engineering Technical Conferences.

[37] Su, H., Collins, C., and McCarthy, J. M., 2002. "An extensible java applet for spatial linkage synthesis". In 2002 ASME Design Engineering Technical Conferences, ASME.

[38] SyMech. http://www.symech.com/.

[39] WATT. http://www.heron-technologies.com.

[40] Sandor, G. N., and Erdman, A. G., 1997. *Advanced Mechanism Design: Analysis and Synthesis Vol. 2*. Prentice-Hall, Englewood Cliffs, NJ.

[41] Suh, C. H., and Radcliffe, C. W., 1978. *Kinematics and Mechanism Design*. Wiley, New York.

[42] McCarthy, J. M., 2000. *Geometric Design of Linkages*. Springer-Verlag, New York.

[43] Farin, G., 1996. *Curves And Surfaces for Computer-Aided Geometric Design: A Practical Guide*, 4th ed. Academic Press, New York.

[44] Hoschek, J., and Lasser, D., 1993. *Fundamentals of Computer Aided Geometric Design*. A K Peters.

[45] Piegl, L., and Tiller, W., 1995. *The NURBS Book*. Springer, Berlin.

[46] Nintendo Wii Motion Control Gaming Platform, http://www.nintendo.com/wii

[47] Microsoft Kinect Motion Control Platform, http://www.xbox.com/en-US/kinect

[48] Eberly, D., 2002. Rotation representations and performance issue. Technical report, Magic Software, Inc.

[49] Rakotomanga, N., Chablat, D., Caro, S., 2008. "Kinetostatic performance of a planar parallel mechanism with variable actuation," In the proceedings of 11th International Symposium on Advances in Robot Kinematics, Kluwer Academic Publishers, Nantes, France.

[50] Arakelian, V., Briot, S., Glazunov, V., 2008. "Increase of singularity-free zones in the workspace of parallel manipulators using mechanisms of variable structure," Mechanism and Machine Theory, **43**(9), pp. 1129–1140

[51] Chablat, D., Wenger, P., 1998. "Working Modes and Aspects in Fully-Parallel Manipulator," In Proceeding IEEE International Conference on Robotics and Automation, pp. 1964–1969.

[52] Wenger, 2004. "Uniqueness domains and regions of feasible paths for cuspidal manipulators," IEEE Transactions on Robotics, **20**(4), pp. 745–750.

[53] Jin, Z., and Ge, Q. J., 2007. "Rational motion interpolation under kinematic constraints of planar 6R closed chain" In ASME 2007 International Design Engineering Technical Conferences & Computers and Information in Engineering Conference, ASME Press. Paper No. DETC2006–99650.

[54] Purwar, A., Jin, Z., and Ge, Q. J., 2008. "Rational motion interpolation under kinematic constraints of spherical 6r closed chains", ASME Journal of Mechanical Design, **130**(6), pp. 0623011 - 0623019.

[55] Purwar, A., Gupta, A., 2011. "Visual Synthesis of RRR- and RPR-Legged Planar Parallel Manipulators using Constraint Manifold Geometry", In ASME 2011 International Design Engineering Technical Conferences & Computers and Information in Engineering Conference, ASME Press. Paper No. DETC2011–48830.

[56] Ge, Q., J., 1990. "Kinematic constraints as algebraic manifolds in the clifford algebra of projective three space", Ph.d. dissertation.

[57] Jin, Z., 2007. "Computer aided synthesis of rational motions under kinematic constraints", Ph.d. dissertation.

[58] Bonev, I., Zlatanov, D., Gosselin, C., 2003. "Singularity Analysis of 3-DOF Planar Parallel Mechanisms via Screw Theory", ASME Journal of Mechanical Design, **125**(9), pp. 573 - 581.

[59] Perez, A., and McCarthy, J., M., 2004. "Dual quaternion synthesis of constraint robotic systems", ASME Journal of Mechanical Design, **126**(3), pp. 425 - 435.

[60] Larochelle, P., and McCarthy, J., M., 1994. "Design of spatial 4c mechanisms for rigid body guidance". In Proc. 1994 ASME Mechanisms Conference, pp. 135 - 142.

[61] Zhao, P., spring 2011. “Formulation of Kinematic Constraints Manifolds in Quaternion Space for Planar Parallel Manipulator”. MEC572 project, Stony Brook University (advised by Prof A. Purwar).

[62] Tsai, L., W., Robot Analysis, the Mechanics of Serial and Parallel Manipulators, John Wiley & Sons, New York, USA, 1999.

[63] Zhang, B., and Crane, C., Special Singularity Analysis for a 6-DOF Parallel Platform”. 10th Int. Conference on Robotics & Remote Systems for Hazardous Environments, Gainesville, FL, USA, 2004.

[64] Mohammadi, Daniali, H., R.,Zsombor-Murray,J., P., and Angeles, J., 1995.”Singularity Analysis of Planar Parallel Manipulators”.Mech. Math. Theory Vol. 30, No. 5, pp. 665-678.

[65] O. Ma and J. Angeles, Int. J. Robotics Automatn 7(1), 23-29 (1992).

[66] Gough, V., E., and Whitehall, S., G., ”Universal Tyre Test Machine,” Proceedings of the FISITA Ninth Int. Technical Congress, London, UK, pp. 117-137, 1962.

[67] Stewart, D., ”A Platform with Six Degrees of Freedom,” Proc of the IMechE, Vol. 180, Pt. 1, No. 15, pp. 371 - 385, 1965-66.

[68] Arsenault, M., and Boudreau, R., 2004. ”The synthesis of Three-Degree-of-Freedom Planar Parallel Mechanisms with Revolute Joints (3-RRR) for an Optimal singulariy-Free Workspace”. Journal of Robotic Systems 21(5), pp. 259 274 .

[69] Carretero, J., A., Podhorodeski, R., P., Nahon, M., A., and Gosselin, C., M., 2000. "Kinematic Analysis of a New Three Degree-of-Freedom spatial Parallel Manipulator", ASME Journal of Mechanical Design, **122**(3), pp. 17 - 24.

[70] Ceccarelli, M., Carbone, G., Ottaviano, E. "An Optimization Problem Approach for Designing both Serial and Parallel Manipulators". Proceedings of MUSME 2005, the International Symposium on Multibody Systems and Mechatronics Uberlandia (Brazil), 6-9 March 2005 Paper no. XX-MUSME05

[71] Williams II, R., Shelley, B., 1997. "Inverse Kinematics for Planar Parallel Manipulators", In ASME 1997 International Design Engineering Technical Conferences, ASME Press. Paper No. DETC97/DAC–3851.

[72] Kim, H., Tsai, L., 2003. "Design Optimization of a Cartesian Parallel Manipulator". *ASME Journal of Mechanical Design,* **125**(3), pp. 43 - 51.

[73] Kim, H., Tsai, L., 2003. "Kinematic Synthesis of a Spatial 3-RPS Parallel Manipulator". *ASME Journal of Mechanical Design,* **125**(3), pp. 92 - 97.

[74] Affi, Z., Romdhane, L., and Maalej, A., 2004. "Dimensional Synthesis of a 3-Translational-DOF in-Parallel Manipulator for a Desired Workspace". *European Journal of Mechanics A/Solids,* **23**, pp. 311 - 324.

[75] Rao, N., Rao, K., 2009. "Dimensional Synthesis of a Spatial 3-RPS Parallel Manipulator for a Prescribed Range of Motion of Spherical Joints". *Journal of Mechanism and Machine Theory,* **44**, pp. 477 - 486.

[76] Kong, X., Gosselin, C., 2008. "Type Synthesis of Six-DOF Wrist-Partioned Parallel Manipulators". *ASME Journal of Mechanical Design,* **130**(6), p. 062302-1.

[77] Angeles, J., 2004. "The Quantitative Synthesis of Parallel Manipulators". *ASME Journal of Mechanical Design,* **126**(7), pp. 617 - 624.

[78] Bai, s., 2010. "Optimum design of spherical parallel manipulators for a prescribed workspace". *Journal of Mechanism and Machine Theory,* **45**, pp. 200 - 211.

[79] Li, Y., Xu, Q., 2006. "Kinematic Analysis and Design of a New 3-DOF Translational Parallel Manipulator". *ASME Journal of Mechanical Design,* **128**(7), pp. 729 - 737.

[80] Jin, Y., Chen, I., and Yang, G., 2009. "Kinematic design of a Family of 6-DOF Partially Decoupled Parallel Manipulators". *Journal of Mechanism and Machine Theory,* **44**, pp. 912 - 922.

[81] Liu, X., Guan, L., and Wang, J., 2007. "Kinematics and Closed Optimal Design of a Kind of PRRRP Parallel Manipulator". *ASME Journal of Mechanical Design,* **129**(5), pp. 558 - 563.

[82] Altuzarra, O., Pinto, C., Sandru, B., Hernandez, A., 2011. "Optimal Dimensioning for Parallel Manipulators: Workspace, Dexterity, and Energy". *ASME Journal of Mechanical Design,* **133**(4), p. 041007-1.